

Is dataset condensation a silver bullet for healthcare data sharing?

Yujiang Wang¹, Anshul Thakur^{1*}, Mingzhi Dong², Pingchuan Ma³, Stavros Petridis³, Li Shang^{2*}, Tingting Zhu¹ and David Clifton⁴

^{1*}Department of Engineering Science, University of Oxford, UK.

^{2*}School of Computer Science, Fudan University, China.

³Department of Computing, Imperial College London, UK.

⁴Oxford Suzhou Centre for Advanced Research (OSCAR), University of Oxford, China.

*Corresponding author(s). E-mail(s):

anshul.thakur@eng.ox.ac.uk; lishang@fudan.edu.cn;

Contributing authors: yujiang.wang@eng.ox.ac.uk;

mingzhidong@gmail.com; pingchuan.ma16@imperial.ac.uk;

stavros.petridis04@imperial.ac.uk; tingting.zhu@eng.ox.ac.uk;

david.clifton@eng.ox.ac.uk;

Abstract

Safeguarding personal information is paramount for healthcare data sharing, a challenging issue without any silver bullet thus far. We study the prospect of a recent deep-learning advent, dataset condensation (DC), in sharing healthcare data for AI research, and the results are promising. The condensed data abstracts original records and irreversibly conceals individual-level knowledge to achieve a bona fide de-identification, which permits free sharing. Moreover, the original deep-learning utilities are well preserved in the condensed data with compressed volume and accelerated model convergences. In PhysioNet-2012, a condensed dataset of 20 samples can orient deep models attaining 80.3% test AUC of mortality prediction (versus 85.8% of 5120 original records), an inspiring discovery generalised to MIMIC-III and Coswara datasets. We also interpret the inhere privacy protections of DC through theoretical analysis and empirical evidence. Dataset condensation opens a new gate to sharing healthcare data for AI research with multiple desirable traits.

Keywords: Healthcare Data Sharing, Dataset Condensation, Mortality Prediction, COVID-19 Diagnosis

1 Introduction

The prevalence of artificial intelligence (AI) in healthcare, especially deep learning, has evolved this field unprecedentedly. With its capability to automate physician processes, deep-learning systems promise to reduce the workloads of clinical practitioners, assist in disease diagnoses and interpretations, improve medical care, and foster patient attendance [1, 2]. Pursuing this favourable landscape of benefiting everyone drives us to accelerate the deployment of deep techniques on clinical grounds. However, deploying healthcare AI is usually challenging and demanding, the “Achilles heel” of which can be ascribed to a simple but persistent issue: the difficulty of obtaining sufficient data for learning.

To be sure, clinical data itself is never an issue. Healthcare digitalisation has led to a dramatically growing number of electronic health records (EHRs) [3], most of which possess valuable clinical knowledge attractive to AI researchers. The chokepoint is the need for a practical approach to sharing them. Clinical data usually comprises sensitive information regarding individuals’ health status. It is paramount to safeguard personal privacy if we want to share it for secondary purposes like AI research, as mandated by laws and ethics.

The classic and common approach for doing so is data anonymisation [4], also called data de-identifications. It is a subtraction-based method that redacts those data fields directly associated with personal identities (“direct identifiers” like names or addresses) and selectively masks out attributes possibly linked with re-identifications (“quasi-identifiers”, e.g. ages and weights), following a particular criterion such as k-anonymity [5] or differential privacy [6, 7]. However, applying this redaction-based anonymisation on high-dimensional datasets like EHRs fails to deliver trustworthy privacy protections, inherently vulnerable to privacy leakages across various scenarios [8–10]. Notably, sharing individual-level data valuable enough for analysis will also inevitably introduce sufficient knowledge for privacy attacks [11]. As a result, there is no silver bullet for privacy-preserving data sharing thus far [12]. A plethora of information-rich clinical datasets harboured in different organisations and institutions remain siloed from public access, significantly detriming the openness of scientific research and hurdling the advents of healthcare AI.

In this work, we aim to place a crucial puzzle to the long-awaited picture of clinical data sharing, deriving from AI fruitions to nurture future healthcare AI research. Originating from dataset distillation study [13], dataset condensation (DC) [14] reaches our vision with various desirable traits for data sharing. The objective of dataset condensation, unlike the regular track of training models, is to learn a “condensed” dataset that can preserve the knowledge

of the original one as much as viable. This condensed dataset can train deep neural networks (DNNs) to operate normally on realistic data points, even though those networks have never learnt from factual data of similar patterns. In computer vision, this method acquires impressive success in condensing a train set of 50,000 images into 500 “fake” ones that still promote DNNs to operate on the test set of 10,000 real-world pictures [14]. Inspiring as it may sound, DC is still an unvisited technique in healthcare. We consider the two distinctive assets that make it a competent candidate for sharing healthcare data, i.e., the inherent privacy protection with well-conserved deep-learning utility and the capability to compress large-scale data for good.

With its unique learning paradigm, DC can irreversibly conceal the individual-level information in the original dataset. DC aims to match the embedding distributions between the original and condensed data computed by DNNs. The parameters of DNNs are not explicitly learnt but are randomly initialised at each training iteration. Two random batches of condensed and original data are then selected to learn the former to match its distributions with the latter in the embedding space of those DNNs. This paradigm is a stone that kills two birds. The knowledge irreversibly flows from original to condensed data via DNNs of randomised parameters operating as innate encrypters. Moreover, matching random original and condensed batches creates a many-to-one correspondence, i.e., each condensed sample can retain knowledge from numerous original instances, which conceals the individual-level information effectively. This unrecoverable record-level concealment allows DC to secure genuine privacy protection and eliminate potential leaks.

Another notable advantage of DC, as indicated by its name, is that it can significantly compress space occupations of clinical datasets to facilitate sharing and storage. More favourably, we can manually control the size of the condensed dataset to satisfy the requirements of diverse scenarios. The condensed dataset can also promote the learning efficiency of DNNs, conveying a faster convergence rate than the original.

This work investigates the prospect of applying DC in sharing healthcare data for the first time. We apply DC to three healthcare datasets of varying clinical variables and tasks to yield condensed versions of train sets. We employ a cohort of 11 DNNs of various architectures to evaluate the original and condensed data utilities for deep learning. We also elaborate on the benefits of condensed data regarding efficient data storage and accelerated model convergence. We then discuss DC’s inherent privacy protection and illustrate the disparate distribution of the condensed data. Finally, although still in its infancy, we show that dataset condensation possesses the potential to rescue us from the groundhog day of de-identification re-identification races, concentrating on sharing knowledge for healthcare AI research.

2 Results

Data. We apply DC to three healthcare datasets to examine DC’s potential in sharing them. The first dataset is denoted as PhysioNet-2012 [15] designed to study the mortality prediction of Intensive Care Unit (ICU) patients, and we analysed the 8,000 publicly-available ICU stays in this work. Each ICU stay consists of up to 42 variables collected at least once during the 48 hours after ICU admission. The target is to predict in-hospital mortalities from those ICU stays. The second dataset, referred to as MIMIC-III [16, 17], contains 21,156 ICU stays of 17 clinical variables collected from the first 48 hours from entering ICU, and the task is predicting in-hospital death for each stay. The last one is named Coswara [18], built for studying the coronavirus (Covid-19) diagnosis from various respiratory sounds. We employ all 1,368 breathing samples and extract acoustic features, aiming to diagnose Covid-19 for each instance.

Across all datasets, we randomly split all original samples into three sets for training, validation, and tests. In PhysioNet-2012, we divide all 8,000 ICU stays into such three sets of 5,120/1,280/1,600 samples, while we group the 21,156 stays from MIMIC-III into 14,698/3,222/3,236 data points. Coswara’s data split yields three sets of 987/175/206 instances, respectively. We thoroughly describe the pre-processing and data splits on three datasets in Supplementary Note 1.

Condensed Data. For each dataset, we learn condensed versions of the train set using dataset condensation as described in Section 4 “Methods”, leaving the validation and test sets untouched for future evaluations. We generate three condensed sets of varying scales per dataset to illustrate the impacts of the number of condensed samples. We condense the train set of PhysioNet-2012 with 5,120 ICU stays into three collections of 20, 40 and 80 data points, respectively. We compress the train set of MIMIC-III (14,698 ICU stays) into sets of 400, 800, and 1,200 instances, while we consolidate the 987 training acoustic features of Coswara into groups of 20, 40, and 80 samples. We observe DNNs’ performances on the test sets when trained on original or condensed sets.

The cohort of DNNs. To examine the generality of condensed data to different neural network architectures, we collect 11 prevalent DNNs for analysing time-series data, most of which have exhibited encouraging performance in the computer vision domain. The cohort consists of three multi-Scale temporal convolution networks (MS-TCNs) [19] with different convolutional kernel sizes, denoted as TCN- α , TCN- β , and TCN- γ ; two vision transformers (ViTs) [20] of distinct attention heads, abbreviated as ViT- α and ViT- β ; two transformer encoders [21] of different attention head numbers and dimensions, referred to as TRSF- α and TRSF- β ; two long short term memory networks (LSTMs) [22] with varying hidden state units, named LSTM- α and LSTM- β ; and two recurrent neural networks (RNNs) [23] of diverse hidden dimensions, dubbed RNN- α and RNN- β . We involve three networks to learn condensed

Table 1: The average performance of DNNs learned on the original train set and three condensed groups on PhysioNet-2012, MIMIC-III, and Coswara datasets. We repeat the training of each DNN five times and compute the mean and standard deviation (SD) of all 11 DNNs. For each data collection, we also report its space consumption in megabytes (MBs).

Datasets	Train data (samples)	Sizes (MBs)	Test AUC (SD)
PhysioNet-2012	Original (5120)	88.13	0.858 (0.011)
	Condensed (80)	0.69	0.804 (0.014)
	Condensed (40)	0.34	0.804 (0.016)
	Condensed (20)	0.17	0.803 (0.012)
MIMIC-III	Original (14698)	322.95	0.840 (0.007)
	Condensed (1200)	13.18	0.756 (0.014)
	Condensed (800)	8.79	0.750 (0.014)
	Condensed (400)	4.39	0.741 (0.019)
Coswara	Original (987)	46.27	0.737 (0.017)
	Condensed (80)	1.88	0.642 (0.016)
	Condensed (40)	0.94	0.641 (0.021)
	Condensed (20)	0.47	0.632 (0.030)

data: TCN- α , ViT- α and LSTM- α , while we deploy all 11 DNNs to evaluate the deep-learning utilities preserved in condensed sets. We outline the architectures and training settings of those DNNs in Supplementary Note 2.

Outcomes. The primary outcome is to investigate DC’s suitability in sharing healthcare data for AI research. We mainly inspect three facets of this vision: 1). the usability of DNNs on realistic data when trained on condensed data, 2). the benefits introduced by DC in terms of data storage and convergence rates, and 3). the inherent privacy protection in condensed data.

Condensed data well preserves deep learning utility with significantly compressed volumes. We expect the condensed data to adequately preserve the deep learning utility of original data for DNNs to operate on realistic samples. To this end, we employ the widely-used area under the curve (AUC) as the primary evaluation metric. We consider the average test AUC of all 11 DNNs trained on the original train sets as the baseline. Then we train the same cohort of DNNs on condensed versions of the same set and study how their test AUC alters from the baseline. To mitigate bias, we repeat the training of each DNN five times and report the average AUC and standard deviation (SD).

We summarise the performance of the original and condensed data across three datasets in Table 1, and we also visualise the results on each dataset in Fig. 1, Fig. 2, and Fig. 3. We enclose the numeric results per DNN in Supplementary Table 8. As shown in Table 1 and Fig. 1c, the original train set of PhysioNet-2012 with 5,120 ICU stays can teach all 11 DNNs to attain an

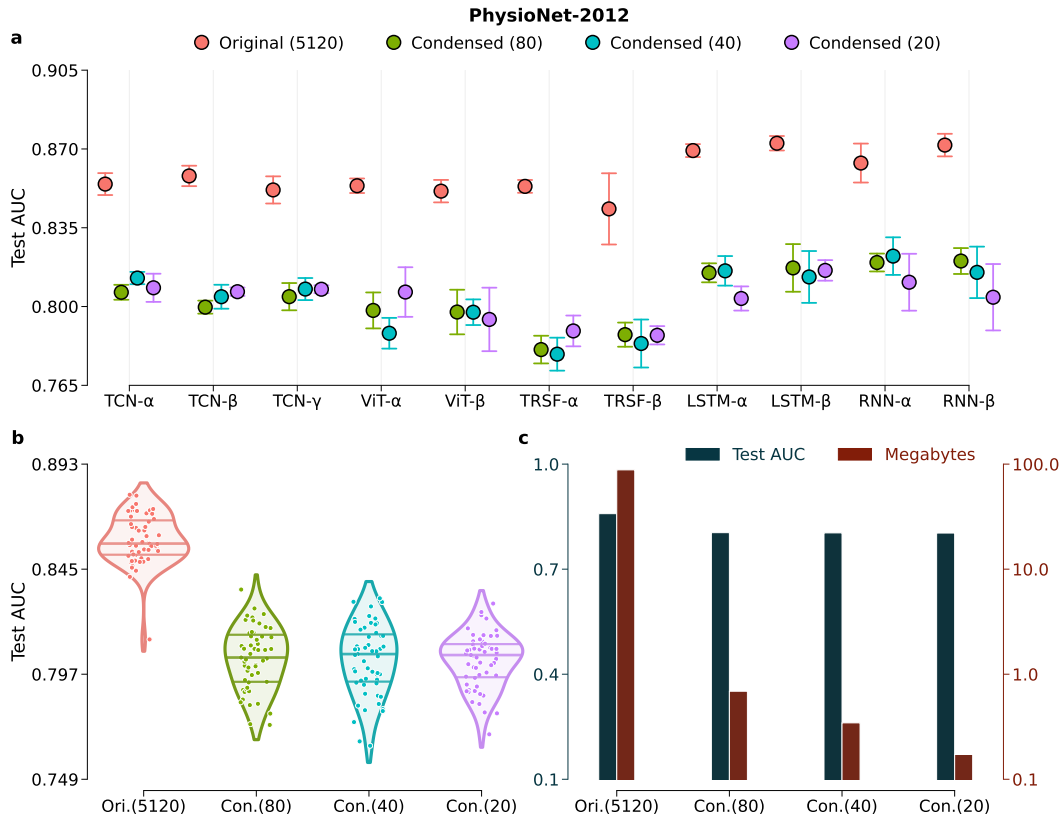


Fig. 1: Visualisations of PhysioNet-2012 results. **a**, The average AUCs across 11 DNNs between the original train set and three scales of condensed data. We post-pend the number of samples to each data group. **b**, The violin plot of all DNNs’ test AUCs across the four data groups. “Ori.” and “Con.” are abbreviations of “Original” and “Condensed”, respectively. **c**, Comparisons of the average AUC and disk space occupation across different data groups. Note that we turn on the logarithm scale to display space usage.

average test AUC = 0.858 (SD 0.011) of predicting in-hospital mortality. Nevertheless, it occupies 88.13 megabytes (MBs) of disk space. On the other hand, DNNs trained on the condensed data of 80, 40, and 20 samples exhibit slightly reduced AUCs = 0.858 \rightarrow 0.804, 0.804, and 0.803, respectively, reflecting an approximate 5.5% drop. Such accuracy costs are arguably acceptable, or even impressive, given the significantly compressed data sizes = 88.13 \rightarrow 0.69, 0.34, and 0.17 MBs, deducting 87.44 MBs (99.2% less than the original) even at the worst case of 80 samples. Besides, the AUCs across three condensed groups are parallel and stable, disregarding the varying number of samples, although the sets of 80 and 40 samples slightly outperform the rest with 20 points. We can also read an interesting phenomenon from the performance comparison of individual DNNs in Fig. 1a. A higher AUC of a certain DNN learnt on the original data will usually accompany better AUCs of the same architecture on the condensed data and vice versa. This tendency can be in line with the mechanism of DC, i.e., matching the embedding distributions between the original

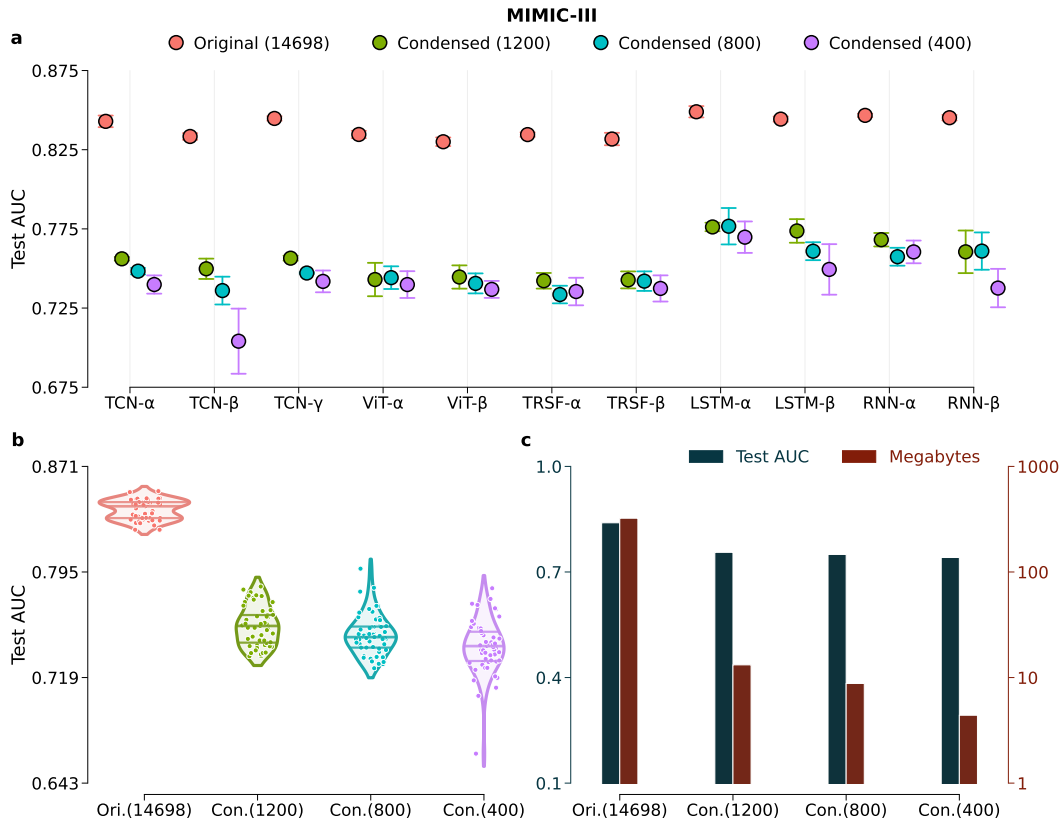


Fig. 2: Visualisations of MIMIC-III results. **a**, The average AUCs across 11 DNNs between the original and three condensed sets. **b**, The violin plot of all DNNs’ test AUCs across the four groups. **c**, Summarizations of AUCs and data sizes across data groups. We turn on the logarithm scale to display space usage.

and condensed data batches, which will likely result in similar embedding patterns for the same DNN structure. In addition, although DNNs other than TCN- α , ViT- α and LSTM- α remain unused during the learning of DC, they can still gain comparable or even better AUCs on the condensed data than the visited three, implying DC’s generalisation capability to a wide variety of neural network architectures.

We can also discover evidence of preserved deep-learning utility from condensed data from MIMIC-III results. As displayed in Table 1 and Fig. 2c, the 11 DNNs learnt on MIMIC-III’s original train set of 14,698 ICU stays can attain a mortality prediction of $\text{AUC} = 0.840$ (SD 0.007), whereas 322.95 MBs space are needed for harbouring the data. Training the same DNNs collection with condensed sets of 1200, 800, and 400 elements yields lower test $\text{AUCs} = 0.840 \rightarrow 0.756, 0.750, \text{ and } 0.741$, respectively. This 8.9% drop in prediction accuracy can be effectively compensated by the considerably relieved storage requirement = $322.95 \rightarrow 13.18, 8.79, \text{ and } 4.39$ MBs, which occupies 95.9%, 97.2%, and 98.6% less space, respectively. The AUC results of individual DNNs

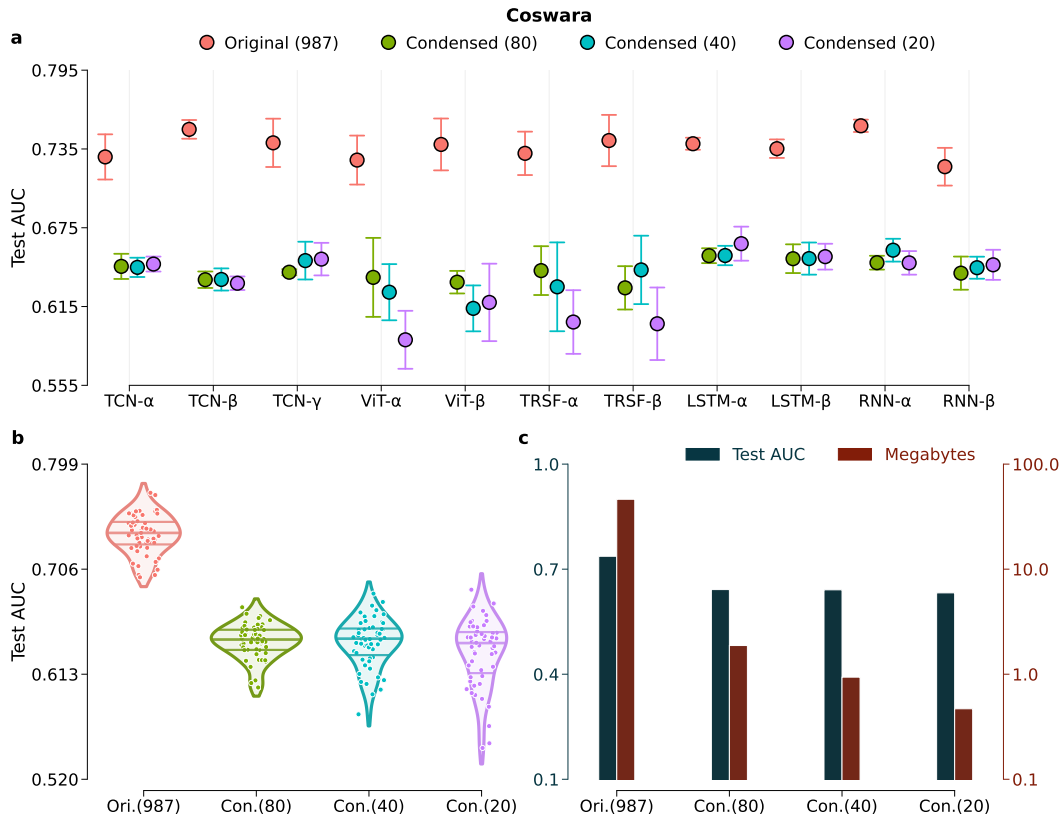


Fig. 3: Visualisations of Coswara results. **a**, The average AUCs across 11 DNNs between the original and three condensed sets. **b**, The violin plot of all DNNs’ test AUCs across the four groups. **c**, Summarizations of AUCs and data sizes across data groups. We turn on the logarithm scale to display space usage.

in Fig. 2a demonstrate a stable AUC correlation between the original and condensed data on the same DNN architectures, a phenomenon consistent with the PhysioNet-2012 results.

On Coswara, we apply DC to a distinct clinical scenario, namely diagnosing Covid-19 from acoustic features of breathing sounds. Considering the achieved DNN accuracy, this task is more formidable than the mortality prediction on PhysioNet-2012 or MIMIC-III. All 11 DNNs learnt with the original train set of 46.27 MBs, as reported in Table 1 and Fig. 3c, can only acquire an average test AUC = 0.737 (SD 0.017), which is less satisfying than that of PhysioNet-2012 or MIMIC-III. Constrained by the AUCs from the original data, the condensed groups of 80, 40, and 20 instances orient DNNs to achieve AUCs = $0.737 \rightarrow 0.642, 0.641, \text{ and } 0.632$, a drop of around 9.6% AUC. DC compresses the disk usage from 46.21 MBs of original into 1.88, 0.94, and 0.47 MBs (80, 40, and 20 condensed instances), respectively, saving 96.0% space. Fig. 3a depicts the AUC comparisons of each architecture, and the overall trend is consistent as in PhysioNet-2012 or MIMIC-III.

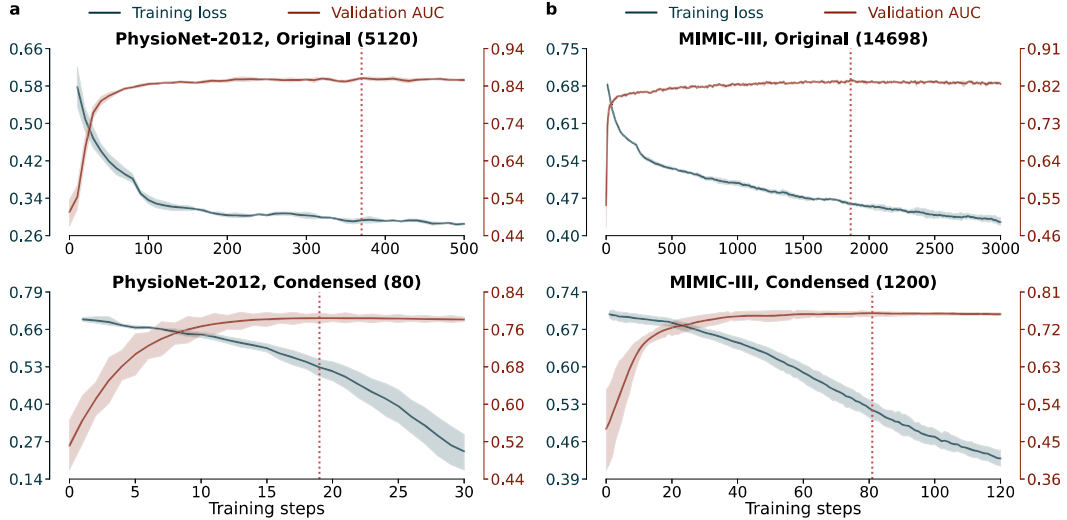


Fig. 4: **a**, The learning curves of TCN- β trained on the original and condensed data of PhysioNet-2012. **b**, The learning curves of TRSF- α trained on the original and condensed data of MIMIC-III. The red-dotted line indicates the step of convergence.

Across three datasets, we can observe that the deep-learning utility of the original data, represented by the average AUC of 11 DNNs, is vastly kept in the condensed data, despite the consolidated volumes and varying clinical scenarios. Notably, the generality of dataset condensation to unseen neural architectures also raises the values of DC for sharing healthcare data.

Table 2: The training steps of convergence across 11 DNNs trained on the original and condensed data. “Ori.” and “Con.” refers to “Original” and “Condensed”, respectively, and “AVG” is the average steps. We post-pend the number of samples to each data group.

Dataset	Train data	Training Steps of Convergence											
		AVG	TCN- α	TCN- β	TCN- γ	ViT- α	ViT- β	TRSF- α	TRSF- β	LSTM- α	LSTM- β	RNN- α	RNN- β
PhysioNet-2012	Ori.(5120)	330	240	370	190	500	340	200	410	170	300	480	440
	Con.(80)	15	7	19	5	2	3	7	6	16	27	33	40
MIMIC-III	Ori.(14698)	3083	4310	4400	3960	2030	1340	1860	2240	2500	3020	3870	4390
	Con.(1200)	273	356	311	361	32	358	81	361	186	323	333	304
Coswara	Ori.(987)	217	148	384	144	132	108	164	104	204	324	324	360
	Con.(80)	26	3	40	25	25	25	40	32	33	24	5	35

Condensed data can lead to a revved convergence of deep models. Sharing the condensed data can introduce another attractive property to AI research: it can accelerate the convergence of DNNs and thus alleviate time costs. To describe this benefit, we plot the learning curves of TCN- β trained on PhysioNet-2012’s original and condensed set in Fig. 4a, and the learnings curves of TRSF- α on MIMIC-III in Fig. 4b, respectively. We can observe from

Fig. 4a that on PhysioNet-2012, it takes approximately 370 training steps for TCN- β to attain convergence (denoted by the red dotted line) on the original train set. The same network trained on 80 condensed samples converges at step = 370 \rightarrow 19, saving 93.1% of training time. Likewise, as shown in Fig. 4b, the average time for TRSF- α to converge in the original MIMIC-III train set is 1,860 training steps, while substantially fewer convergence steps = 1,860 \rightarrow 81 are required on the condensed set of 1200 instances, which accelerates the training session by 95.6%. We enclose the learning curves of addition networks in Supplementary Note 3.

We deliver a detailed comparison of the convergence steps between the original and condensed data of each DNN in Table 2. It can be discovered that accelerated learning of condensed data is a common trait across all datasets and networks. On average, the condensed data can boost the training speed by 95.4%, 91.1%, and 88.0% than the original on PhysioNet-2012, MIMIC-III, and Coswara, respectively. Consequently, sharing condensed data can benefit healthcare AI research with significantly compacted volume and faster model learning. Such traits can be highly desirable when sharing a dataset of massive data volumes that can be time-consuming to complete the model training.

Condensed data effectively conceals individual-level knowledge.

The innate privacy protections are the most attractive property of DC, aside from the well-preserved ML utility and compressed data volume. As described in Section 4, DC performs distributions matching between two random batches of original and condensed data embedded by randomised DNNs. Since the number of condensed samples is far less than the original, this mechanism creates a many-to-one correspondence. Each condensed sample receives knowledge from multiple original instances, and the condensed set is essentially a macro-level synthesis of the original dataset. From this perspective, sharing a condensed dataset is comparable to sharing the metadata, such as the mean and STD of clinical variables, which hides individual-level information and is thus permitted by relevant regulations.

To illustrate this privacy-preserving property, we visualise in Fig. 5a six data examples randomly chosen from the MIMIC-III and its condensed set as 2D heatmaps. The heatmaps of original instances exhibit highly-regulated and potentially-identifiable patterns, representing a potential threat of privacy leaks. In contrast, the heatmaps of condensed samples display patterns of complete chaos, indicating that they are essentially random signals without any explicit meaning. Those unorganised signals result from the learning of DC; each condensed instance receives and fuses the knowledge of multiple original samples. As a result, original data of organised patterns are entangled and randomised into samples of chaotic signals, which can arguably safeguard the personal information in healthcare data.

We further investigate this issue by examining various clinical variables. Fig. 5b depicts the 48-hour trends of six clinical variables computed from 80 original and 80 condensed samples of PhysioNet-2012. Those variables

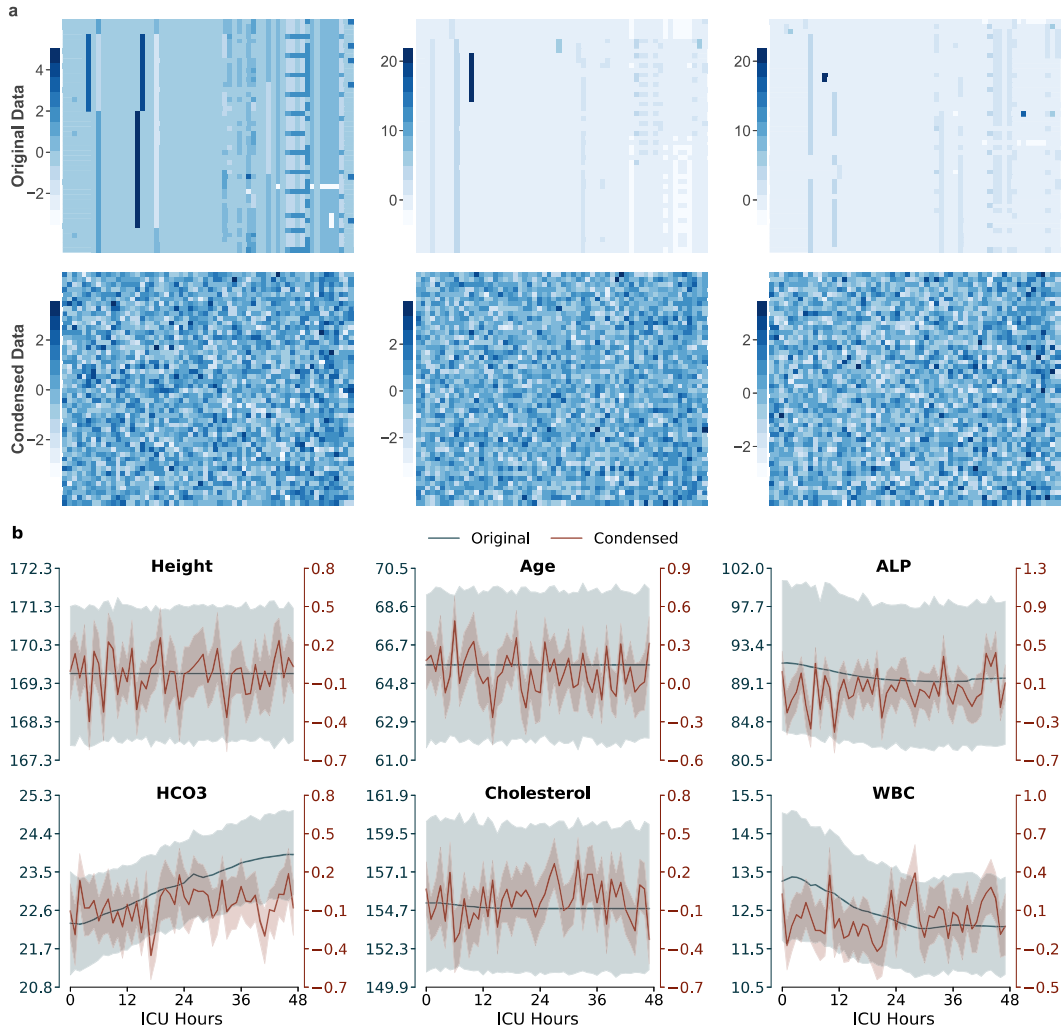


Fig. 5: Visualisations of original and condensed samples. **a**, the heatmaps of three original and three condensed samples randomly drawn from MIMIC-III. **b**, the 48-hour trends of six clinical variables from PhysioNet-2012 computed from 80 original and 80 condensed instances, respectively.

are: “height”, “age”, “alkaline phosphatase” (“ALP”), “serum bicarbonate” (“HCO3”), “cholesterol”, and “white blood cell count” (“WCB”). As general descriptors, “height” and “age” from the original samples demonstrate constant values across the ICU period. However, the same variables from the condensed data show significantly fluctuating trends over time, which is improbable in real cases and can shield the variable-level information. We can observe similar deviations between the rest original and condensed variables. For instance, the overall value of the original “ALP” and “WCB” declines as hours increase, while their condensed curves display an inconsistent trend with randomised noises. Fluctuations on condensed variables can be discovered on “HCO3” with an increasing tendency in the original. We can notice that irregular fluctuations of variables are common traits of condensed samples, despite the conceivably regular patterns in the original

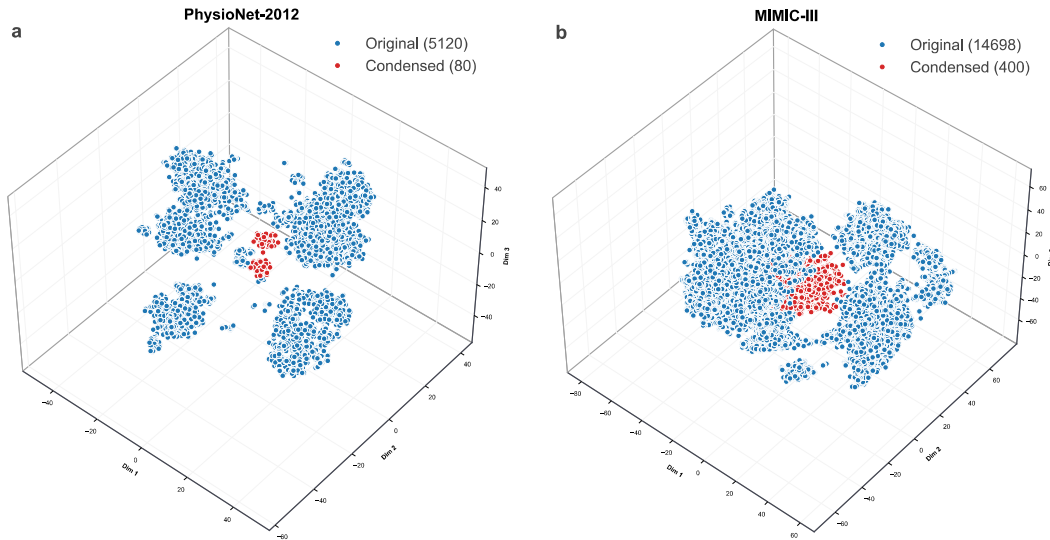


Fig. 6: The visualisations of the original and condensed samples embedded into 3D with t-SNE. **a**, the 3D distributions of 5,120 original and 80 condensed samples of PhysioNet-2012. **b**, the 3D distributions of 14,698 original and 400 condensed samples of MIMIC-III.

variables. Such observations are consistent with the heatmap visualisation of Fig. 5a and reflect inherent protections at the clinical variable level. Besides, each variable range is automatically shifted and rescaled into arbitrary fields approximately between -1 and 1 , further encrypting variable-level knowledge to attain better privacy protections. We supplement more comparisons of original and condensed samples in Supplementary Note 3.

The distribution of condensed data is disparate from the original.

Concealments at individual and variable levels can imply a potential disparate distribution in condensed data that effectively hides the realistic data distribution from potential attacks. Sharing condensed data is, therefore, sharing an unseen dataset independent from the original. To explain this distribution shifting, we apply t-distributed stochastic neighbour embedding (t-SNE) [24] to visualise the 3D distributions of the original and condensed data of PhysioNet-2012 in Fig. 6a and MIMIC-III in Fig. 6b. PhysioNet-2012’s original data points loosely constitute four distant clusters as in Fig 6a, leaving an unoccupied heart region. On the other hand, the condensed points exhibit a deviating distribution. Most of them reside within the central but empty region that separates the original clusters, and we observe only two distinctive groups. Such distribution can result from the many-to-one correspondence in DC. Since each condensed point receives information from multiple original samples, their distribution naturally moves to the central region that best balances the knowledge from different cases. From this perspective, the condensed data substantively reflects the macro-level information of the original dataset, and sharing them is just like sharing statistical data such as mean or

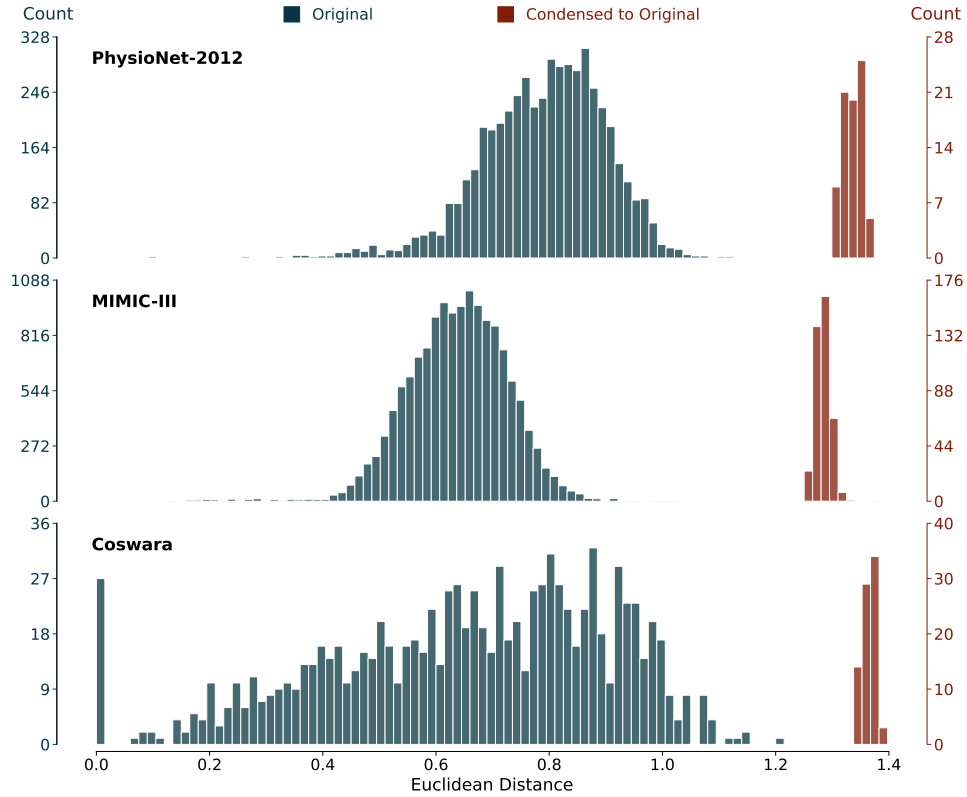


Fig. 7: The distance histograms of PhysioNet-2012, MIMIC-III, and Coswara. For each condensed sample, we find its minimum euclidean distance with every original instance and plot the minimum distances of all condensed samples as the histogram (“Condensed to Original” in red). For each original sample, we find its minimum Euclidean distance with every other instance and plot the histogram for all original ones (“Original” in blue).

STD. We can see from Fig 6b that the distributions between the original and condensed on MIMIC-III are also in line with this analysis. Despite the significantly increased density, MIMIC-III’s original data constitute several clusters with a sparse central area in which all condensed points reside, indicating the macro-level essence of condensed data.

We further inspect the distribution shifting by computing euclidean distances between samples. We plot in Fig. 7 the histogram of euclidean distances within the original train sets and the distance histogram from the condensed instances to the original, respectively. Across all three datasets, the distances within the original data are significantly less than those from condensed to the original. For example, the distances between most MIMIC-III original samples fall between 0.4 and 0.9, while the distances from condensed instances to the original ones significantly increased to the scope of 1.3 and 1.4. In other words, any condensed-to-original distance is around two times longer than the original-to-original, indicating that condensed points inhabit space distant from the original span. Similar distribution divergences can also be observed

from the histograms of PhysioNet-2012 and Coswara in Fig. 7, in which the distances between condensed and original samples significantly surpass those between original ones. With the shifted distribution, sharing condensed data can prevent privacy leaks that persist in sharing individual-level data of realistic distributions.

3 Discussion

Data sharing stands at the heart of fostering innovations in healthcare AI research; however, lacking a satisfactory privacy-preserving sharing mechanism is a long-haunted issue that detracts its development. This paper examines the potential of dataset condensation, a recent AI fruition, in sharing healthcare data for AI research. The experimental results on three healthcare datasets, PhysioNet-2012, MIMIC-III, and Coswara, reveal that DC can preserve the deep-learning utility in the original clinical records and simultaneously facilitate sharing with the compressed data volume. Condensed data can also teach DNNs to converge at much faster paces, significantly reducing training costs. The inherent privacy protection, an attractive property of DC, is also analysed and discussed. Condensed data irreversibly conceals individual-level information and prevents potential privacy leaks with the many-to-one learning mechanism and disparate distributions. As macro-level information, condensed data can be shared just like metadata. The prospect of DC is promising. It may free us from the unceasing races between de-identifications and re-identifications, focusing on sharing AI-oriented knowledge for deep learning research. Data holders of clinical datasets of highly sensitive but also valuable knowledge can apply DC to learn a condensed set to be freely shared without privacy concerns. Healthcare researchers can also share the condensed version of their private datasets that are usually time-consuming or impossible to receive access approvals. Other researchers can use condensed datasets of significantly compressed sizes to train less accurate but still workable DNNs at accelerated convergence rates. Although still in its infancy, DC can present inspiring outlooks of facilitating scientific studies' openness and promoting AI research in healthcare.

On the other hand, dataset condensation has various limitations, and we elaborate on them following the *no free lunch* view in [25]. Any method of sharing data with privacy protections comes at a cost, typically impaired data utility. Classic anonymisation approaches attain de-identification by redacting direct and quasi-identifiers, leading to a degradation in the data utility. Removing more data fields will generally lead to better privacy protection but at the cost of further demolished usability. This trade-off between privacy and data utility can also be applied to sharing synthetic data acquired with generative adversarial networks (GANs) [26, 27]. As portrayed in [25], high-level privacy protection in synthetic data comes at the price of deteriorated usability, and vice versa for retaining good data utility and increased vulnerability to privacy attacks. Besides, drawn from a realistic data distribution, synthetic data

possesses individual-level information of original samples; hence, the potential privacy leaks persist.

The *no free lunch* view also retains for DC. Condensed data is essentially macro-level descriptors of the original dataset, concealing individual-level information to achieve a bona fide de-identification. However, hiding such knowledge also eliminates data usability at fine-grained scales crucial to exploiting the full value of clinical records. Condensed data can be of limited profit for analytical tasks that demand access to microdata, and this is one of the major costs for DC's inherent privacy protections. Also, the compressed data volume that facilitates sharing and model learning docks at the expense of inevitable information losses, represented by the degraded prediction accuracy in learnt DNNs. There is no free lunch in privacy-preserving sharing, and we must review the pros and cons simultaneously. Despite the annihilated individual-level utility, the most attractive merit of DC is that it permits the sharing of AI-oriented knowledge free of privacy concerns, which could potentially revolutionise the field. Healthcare AI research can profoundly benefit from open-access condensed data of those clinical datasets that are usually difficult to be shared directly.

Eventually, we consider dataset condensation as a newly-emerged and encouraging data-sharing route for deploying healthcare AI. There were approximately three categories of privacy-preserving sharing mechanisms before DC: 1). the classic redaction-based data anonymisation [4], 2). the GAN-generated synthetic data sharing [25], and 3). remote-processing systems for delivering population-level insights such as secure multiparty computation or homomorphic encryption [28]. DC reveals an unvisited avenue with unique advantages. Individual-level knowledge within anonymised or synthetic data represents an inevitable chance of privacy breach. They also face the quagmire of finding a satisfying trade-off between security and utility. On the other hand, DC is free of privacy concerns and represents greater sharing flexibility, and applying DC is also more straightforward without security-utility balancing steps. DC also differs from those remote-processing systems in multiple aspects. Building those remote systems can be costly and time-consuming, including hardware setup, daily maintenance, framework construction, etc. After being built, those systems could only support pre-defined analytical tasks and lacked the flexibility to adapt to learning models of varying architectures. DC, in contrast, is a low-cost and easy-to-implement technique, and we can deploy it to output condensed data directly and swiftly (see Supplementary Table 10 for the required learning time). The well-preserved deep learning utility in condensed data also significantly distinguishes DC from remote systems like homomorphic encryption.

To sum up, since there is no free lunch in sharing privacy-sensitive data, there is no silver bullet that can simultaneously attain perfect privacy protection and flawless data utility. Dataset condensation, however, can be a promising technique for sharing AI-oriented knowledge to benefit healthcare AI research with its unique properties.

4 Methods

Problem definition. We define the original train set of a healthcare dataset as $\mathcal{O} = \{(\mathbf{x}_i, y_i) \mid 1 \leq i \leq |\mathcal{O}|\}$ where $\mathbf{x}_i \in \mathbb{R}^{T \times F}$ is the i -th time-series sample with T and F as the temporal and feature dimension, respectively, y_i is the class label, and $|\mathcal{O}|$ refers to the total number of samples. where $\mathbf{c}_i \in \mathbb{R}^{T \times F}$ is a condensed sample, $|\mathcal{C}|$ is the number of condensed samples, and $|\mathcal{C}| \ll |\mathcal{O}|$. We expect that \mathcal{C} can preserve the deep-learning utility in \mathcal{O} such that when replacing the train set \mathcal{O} with \mathcal{C} , DNNs can still achieve parallel performance on an unseen test set, which can be denoted as

$$\mathbb{E}_{\mathbf{x} \sim P_{\mathcal{D}}}[\mathbb{L}(\varphi_{\theta^{\mathcal{O}}}(\mathbf{x}), y)] \simeq \mathbb{E}_{\mathbf{x} \sim P_{\mathcal{D}}}[\mathbb{L}(\varphi_{\theta^{\mathcal{C}}}(\mathbf{x}), y)]. \quad (1)$$

In Eq. 1, $\mathbf{x} \in \mathbb{R}^{T \times F}$ is a data sample drawn from the original data distribution $P_{\mathcal{D}}$, y is the class label, \mathbb{L} is a loss function such as the binary cross-entropy (BCE), φ is a DNN with parameters θ , $\varphi_{\theta^{\mathcal{O}}}$ and $\varphi_{\theta^{\mathcal{C}}}$ denote the DNN trained on \mathcal{O} and \mathcal{C} , respectively. Eq. 1 is DC’s objective for time-series healthcare data; however, it is challenging to optimise this equation directly. We follow [14] to solve Eq. 1, seeking to match the distributions in embedding spaces which are more efficient to compute.

Dataset condensation with distribution matching. The major challenge of optimising Eq. 1 is the estimation of data distribution $P_{\mathcal{D}}$. Considering the high-dimensional healthcare samples, obtaining an accurate and reasonable $P_{\mathcal{D}}$ can be computationally expensive and practically infeasible. To address the same issue in computer vision, authors of [14] assume that each image sample can be embedded into a lower-dimensional space with a group of parametric functions and then assemble results to estimate the original image data distributions. In this work, we obey the same premise for healthcare data, embedding each sample $\mathbf{x} \in \mathbb{R}^{T \times F}$ with a collection of parametric functions $\phi_{\mu} : \mathbb{R}^{T \times F} \mapsto \mathbb{R}^{T' \times F'}$ where $T' \ll T$, $F' \ll F$, and μ stands for the parameters of a function ϕ . Each ϕ_{μ} reveals a fragment of the original sample distribution while merging them together can provide a reasonable $P_{\mathcal{D}}$ estimation.

Under this landscape, we can match embeddings between the original and condensed datasets using the maximum mean discrepancy (MMD) distances [29], which can be described as

$$\sup_{\|\phi_{\mu}\|_{\mathcal{H}} \leq 1} (\mathbb{E}[\phi_{\mu}(\mathcal{O})] - \mathbb{E}[\phi_{\mu}(\mathcal{C})]) \quad (2)$$

where \mathcal{H} represents the reproducing kernel Hilbert space (RKHS). We employ an empirical estimation of MMD distance in Eq. 2 following [14], which can be written as

$$\mathbb{E}_{\mu \sim P_{\mu}} \left\| \frac{1}{|\mathcal{O}|} \sum_{i=1}^{|\mathcal{O}|} \phi_{\mu}(\mathbf{x}_i) - \frac{1}{|\mathcal{C}|} \sum_{j=1}^{|\mathcal{C}|} \phi_{\mu}(\mathbf{c}_j) \right\|^2 \quad (3)$$

where P_{μ} refers to the parameter distribution of ϕ_{μ} .

There are different methods for embedding networks $\phi_{\boldsymbol{\mu}}$. The authors of [14] took a fixed network architecture and sampled randomised parameters at each training step. We extend this approach to a group of network architectures in pursuit of better structural generalisations and privacy protections. For each training step, we first randomly pick a network $\phi_{\boldsymbol{\mu}_i}^i$ from a collection $\Phi = \{\phi_{\boldsymbol{\mu}_i}^i \mid 1 \leq i \leq |\Phi|\}$ where $\phi_{\boldsymbol{\mu}_i}^i$ denotes the i -th DNN with parameters $\boldsymbol{\mu}_i$ and $|\Phi|$ denotes the collection size. We generate randomised weights from parameter distribution $P_{\boldsymbol{\mu}_i}$ for the selected network. This dual-sampling strategy turns the objective into an optimisation issue that can be described as

$$\min_{\mathcal{C}} \mathbb{E}_{\phi_{\boldsymbol{\mu}_k}^k \sim \Phi, \boldsymbol{\mu}_k \sim P_{\boldsymbol{\mu}_k}} \left\| \frac{1}{|\mathcal{O}|} \sum_{i=1}^{|\mathcal{O}|} \phi_{\boldsymbol{\mu}_k}^k(\mathbf{x}_i) - \frac{1}{|\mathcal{C}|} \sum_{j=1}^{|\mathcal{C}|} \phi_{\boldsymbol{\mu}_k}^k(\mathbf{c}_j) \right\|^2. \quad (4)$$

Eq. 4 states that we would like to learn a condensed dataset \mathcal{C} that can minimise the discrepancy between the two distributions of original and condensed data in the embedding spaces projected by an arbitrary network $\phi_{\boldsymbol{\mu}_k}^k$ with randomly-sampled parameters $\boldsymbol{\mu}_k$.

The randomised network architecture and parameters are probably one of the most interesting mechanisms of DC. At first glance, it may be counter-intuitive how a randomised network of randomised parameters can lead to a proper embedding of original data, and we may also suspect how the deep-learning knowledge can flow from the original to the condensed dataset smoothly. Relevant study [30], however, indicates that randomly-initialised networks can extract feature descriptors of high qualities for various computer vision tasks. Those networks can also maintain the distance affinity of original samples in the embedding spaces, e.g., the embedding distance of two samples of the same category is less than those of different classes, as demonstrated in [31]. With high-quality and distance-preserving representations, we can expect randomly-initialised DNNs to construct a meaningful distribution of original data in the embedding space, which can adequately guide the learning of the condensed dataset. Applying this randomised-network strategy can also yield a favourable trait in healthcare: the irreversible knowledge flow from original to condensed data. It is computationally impossible to trace back to any original data from the condensed dataset without knowing network $\phi_{\boldsymbol{\mu}_k}^k$ and sampled parameters $\boldsymbol{\mu}_k$ that are forgotten after training of DC.

Learning the condensed dataset. To learn the condensed dataset \mathcal{C} in Eq. 4, we employ a mini-batch training algorithm as in [14]. We first randomly initialised a condensed dataset \mathcal{C} , which is learnt for a total of M iterations. For each iteration, we perform randomised samplings as follows: 1). sample a network $\phi_{\boldsymbol{\mu}_k}^k \sim \Phi$, 2). sample this network’s parameters $\boldsymbol{\mu}_k \sim P_{\boldsymbol{\mu}_k}$, 3). for each class s , sample an original data batch $B_s^{\mathcal{O}} \sim \mathcal{O}$ and a condensed data batch $B_s^{\mathcal{C}} \sim \mathcal{C}$. The average discrepancy between original and condensed data batches across all classes is computed as the loss \mathcal{L} at this iteration, which can

Algorithm 1 Learning a condensed healthcare dataset

Input: The original healthcare dataset \mathcal{O} **Require:** The randomly-initialised condensed dataset \mathcal{C} with $|\mathcal{C}|$ samples of S classes, the collection of deep networks Φ , the parameter distribution P_{μ_k} for arbitrary network in Φ , the training iterations M , the learning rate ξ

- 1: **for** $m = 1 : M$ **do**
- 2: Sample network $\phi_{\mu_k}^k \sim \Phi$
- 3: Sample network parameters $\mu_k \sim P_{\mu_k}$
- 4: **for** $s = 1 : S$ **do**
- 5: Sample an original batch $B_s^{\mathcal{O}} \sim \mathcal{O}$
- 6: Sample a condensed batch $B_s^{\mathcal{C}} \sim \mathcal{C}$
- 7: **end for**
- 8: Compute loss \mathcal{L} as in Eq. 5
- 9: Update $\mathcal{C} \leftarrow \mathcal{C} - \xi \nabla_{\mathcal{C}} \mathcal{L}$
- 10: **end for**

Output: The condensed healthcare dataset \mathcal{C}

be written as

$$\mathcal{L} = \sum_{s=1}^S \left\| \frac{1}{|B_s^{\mathcal{O}}|} \sum_{(\mathbf{x}, y) \in B_s^{\mathcal{O}}} \phi_{\mu_k}^k(\mathbf{x}) - \frac{1}{|B_s^{\mathcal{C}}|} \sum_{(\mathbf{c}, y) \in B_s^{\mathcal{C}}} \phi_{\mu_k}^k(\mathbf{c}) \right\|^2 \quad (5)$$

where S denotes the total classes in \mathcal{O} . Eventually, we use the stochastic gradient descent (SGD) algorithm to update the condensed dataset \mathcal{C} w.r.t the loss \mathcal{L} , which can be denoted as $\mathcal{C} \leftarrow \mathcal{C} - \xi \nabla_{\mathcal{C}} \mathcal{L}$ where ξ is the learning rate. We depict the training process in Algorithm 1.

Eq. 5 illustrates the many-to-one correspondences between original and condensed samples. Since $|\mathcal{C}| \ll |\mathcal{O}|$, each sample in the condensed batch $B_s^{\mathcal{C}}$ will be exposed to numerous original instances of the same class during training iterations, indicating a mixture of knowledge from multiple cases. This macro-level understanding effectively conceals individual-level information in original data, leading to a ‘‘bona fide’’ de-identification.

Hyper-parameters. Across all three datasets, we apply an Adam [32] optimiser with an initial learning rate of 0.001 to update \mathcal{C} as operation 9 of Algorithm 1, and we train every condensed dataset for a total of 24,000 iterations. The batch size of $B_s^{\mathcal{O}}$ and $B_s^{\mathcal{C}}$ is uniquely set to be 256. On PhysioNet-2012 and Coswara, we generate three condensed datasets of different samples, i.e., $|\mathcal{C}| = 20, 40, \text{ and } 80$, while we set the sizes $|\mathcal{C}|$ of MIMIC-III to be 400, 800, and 1,200, respectively. We randomly initialise each condensed dataset from scratch and set the proportions of positive and negative labels to be 50% and 50%. In this work, we set the collection Φ to consist of three network architectures, namely TCN- α , ViT- α , and LSTM- α . We also explore

the effects of varying temporal dimensions in condensed samples (see Supplementary Table 9).

Declarations

Data availability. The data used in this study are freely and publicly available. The PhysioNet-2012 dataset can be accessed at <https://physionet.org/content/challenge-2012/1.0.0/>. The MIMIC-III dataset can be accessed at <https://physionet.org/content/mimiciii/1.4/>. The Coswara dataset can be accessed at <https://github.com/iiscleap/Coswara-Data>.

Acknowledgements. This work was supported in part by the National Institute for Health Research (NIHR) Oxford Biomedical Research Centre (BRC), and in part by an InnoHK Project at the Hong Kong Centre for Cerebro-cardiovascular Health Engineering). D.C. is an Investigator in the Pandemic Sciences Institute, University of Oxford, Oxford, UK. Y.W. is supported by an NIHR Healthcare Technologies Award (project number NIHR131227) and by an MRC research grant (MR/W01761X/1). A.T. is supported by an EPSRC Healthcare Technologies Challenge Award (EP/N020774/1). The views expressed are those of the authors and not necessarily those of the NHS, the NIHR, the MRC, the Department of Health, InnoHK – ITC, or the University of Oxford.

Authors' contributions. Y.W. conducted the data analysis and prepared the manuscript. A.T. checked the validity of the data and performed pre-processing. A.T., M.D., L.S., T.Z., and D.C. conceived and devised the study. P.M. and S.P. implemented MS-TCN architectures. All authors contributed to the results discussion and final manuscript preparation.

Competing interests. The authors declare no competing interests.

References

- [1] Topol, E.J.: High-performance medicine: the convergence of human and artificial intelligence. *Nature medicine* **25**(1), 44–56 (2019)
- [2] Zhang, A., Xing, L., Zou, J., Wu, J.C.: Shifting machine learning for healthcare from development to deployment and from models to data. *Nature Biomedical Engineering*, 1–16 (2022)
- [3] Rajkomar, A., Oren, E., Chen, K., Dai, A.M., Hajaj, N., Hardt, M., Liu, P.J., Liu, X., Marcus, J., Sun, M., *et al.*: Scalable and accurate deep learning with electronic health records. *NPJ digital medicine* **1**(1), 1–10 (2018)

- [4] El Emam, K., Arbuckle, L.: *Anonymizing Health Data: Case Studies and Methods to Get You Started*, 1st edn. O'Reilly Media, Inc., Sebastopol (2013)
- [5] Samarati, P., Sweeney, L.: *Protecting privacy when disclosing information: k-anonymity and its enforcement through generalization and suppression* (1998)
- [6] Dwork, C.: *Differential privacy: A survey of results*. In: *International Conference on Theory and Applications of Models of Computation*, pp. 1–19 (2008). Springer
- [7] Dwork, C., Roth, A., *et al.*: *The algorithmic foundations of differential privacy*. *Foundations and Trends® in Theoretical Computer Science* **9**(3–4), 211–407 (2014)
- [8] De Montjoye, Y.-A., Radaelli, L., Singh, V.K., Pentland, A.S.: *Unique in the shopping mall: On the reidentifiability of credit card metadata*. *Science* **347**(6221), 536–539 (2015)
- [9] Narayanan, A., Shmatikov, V.: *Myths and fallacies of “personally identifiable information”*. *Communications of the ACM* **53**(6), 24–26 (2010)
- [10] Sweeney, L., Yoo, J.S.: *De-anonymizing south korean resident registration numbers shared in prescription data*. *Technology Science* (2015)
- [11] Narayanan, A., Shmatikov, V.: *Robust de-anonymization of large sparse datasets: a decade later* (2019)
- [12] Stadler, T., Troncoso, C.: *Why the search for a privacy-preserving data sharing mechanism is failing*. *Nature Computational Science* **2**(4), 208–210 (2022)
- [13] Wang, T., Zhu, J.-Y., Torralba, A., Efros, A.A.: *Dataset distillation*. arXiv preprint arXiv:1811.10959 (2018)
- [14] Zhao, B., Bilen, H.: *Dataset condensation with distribution matching*. *CoRR* **abs/2110.04181** (2021) <https://arxiv.org/abs/2110.04181>
- [15] Silva, I., Moody, G., Scott, D.J., Celi, L.A., Mark, R.G.: *Predicting in-hospital mortality of icu patients: The physionet/computing in cardiology challenge 2012*. In: *2012 Computing in Cardiology*, pp. 245–248 (2012). IEEE
- [16] Johnson, A.E., Pollard, T.J., Shen, L., Lehman, L.-w.H., Feng, M., Ghassemi, M., Moody, B., Szolovits, P., Anthony Celi, L., Mark, R.G.: *Mimic-iii, a freely accessible critical care database*. *Scientific data* **3**(1),

1–9 (2016)

- [17] Johnson, A., Pollard, T., Mark, R.: Mimic-iii clinical database (version 1.4). *PhysioNet* **10**, 2–26 (2016)
- [18] Sharma, N., Krishnan, P., Kumar, R., Ramoji, S., Chetupalli, S., Nirmala, R., Kumar Ghosh, P., Ganapathy, S.: Coswara-a database of breathing, cough, and voice sounds for covid-19 diagnosis. In: *Proceedings of the Annual Conference of the International Speech Communication Association, INTERSPEECH*, vol. 2020, pp. 4811–4815 (2020). International Speech Communication Association
- [19] Martinez, B., Ma, P., Petridis, S., Pantic, M.: Lipreading using temporal convolutional networks. In: *ICASSP 2020-2020 IEEE International Conference on Acoustics, Speech and Signal Processing (ICASSP)*, pp. 6319–6323 (2020). IEEE
- [20] Dosovitskiy, A., Beyer, L., Kolesnikov, A., Weissenborn, D., Zhai, X., Unterthiner, T., Dehghani, M., Minderer, M., Heigold, G., Gelly, S., Uszkoreit, J., Houlsby, N.: An image is worth 16x16 words: Transformers for image recognition at scale. In: *International Conference on Learning Representations* (2021). <https://openreview.net/forum?id=YicbFdNTTy>
- [21] Vaswani, A., Shazeer, N., Parmar, N., Uszkoreit, J., Jones, L., Gomez, A.N., Kaiser, L., Polosukhin, I.: Attention is all you need. *Advances in neural information processing systems* **30** (2017)
- [22] Hochreiter, S., Schmidhuber, J.: Long short-term memory. *Neural computation* **9**(8), 1735–1780 (1997)
- [23] Hopfield, J.J.: Neural networks and physical systems with emergent collective computational abilities. *Proceedings of the national academy of sciences* **79**(8), 2554–2558 (1982)
- [24] Van der Maaten, L., Hinton, G.: Visualizing data using t-sne. *Journal of machine learning research* **9**(11) (2008)
- [25] Stadler, T., Oprisanu, B., Troncoso, C.: Synthetic data–anonymisation groundhog day. In: *31st USENIX Security Symposium (USENIX Security 22)*, pp. 1451–1468 (2022)
- [26] Goodfellow, I., Pouget-Abadie, J., Mirza, M., Xu, B., Warde-Farley, D., Ozair, S., Courville, A., Bengio, Y.: Generative adversarial networks. *Communications of the ACM* **63**(11), 139–144 (2020)

- [27] Xu, L., Skoularidou, M., Cuesta-Infante, A., Veeramachaneni, K.: Modeling tabular data using conditional gan. *Advances in Neural Information Processing Systems* **32** (2019)
- [28] Froelicher, D., Troncoso-Pastoriza, J.R., Raisaro, J.L., Cuendet, M.A., Sousa, J.S., Cho, H., Berger, B., Fellay, J., Hubaux, J.-P.: Truly privacy-preserving federated analytics for precision medicine with multiparty homomorphic encryption. *Nature communications* **12**(1), 1–10 (2021)
- [29] Gretton, A., Borgwardt, K.M., Rasch, M.J., Schölkopf, B., Smola, A.: A kernel two-sample test. *The Journal of Machine Learning Research* **13**(1), 723–773 (2012)
- [30] Saxe, A.M., Koh, P.W., Chen, Z., Bhand, M., Suresh, B., Ng, A.Y.: On random weights and unsupervised feature learning. In: *Icml* (2011)
- [31] Giryes, R., Sapiro, G., Bronstein, A.M.: Deep neural networks with random gaussian weights: A universal classification strategy? *IEEE Transactions on Signal Processing* **64**(13), 3444–3457 (2016)
- [32] Kingma, D.P., Ba, J.: Adam: A method for stochastic optimization. *arXiv preprint arXiv:1412.6980* (2014)

Supplementary Information - Is dataset condensation a silver bullet for healthcare data sharing?

Yujiang Wang¹, Anshul Thakur^{1*}, Mingzhi Dong², Pingchuan Ma³, Stavros Petridis³, Li Shang^{2*}, Tingting Zhu¹ and David Clifton⁴

^{1*}Department of Engineering Science, University of Oxford, UK.

^{2*}School of Computer Science, Fudan University, China.

³Department of Computing, Imperial College London, UK.

⁴Oxford Suzhou Centre for Advanced Research (OSCAR),
University of Oxford, China.

*Corresponding author(s). E-mail(s):

anshul.thakur@eng.ox.ac.uk; lishang@fudan.edu.cn;

Contributing authors: yujiang.wang@eng.ox.ac.uk;

mingzhidong@gmail.com; pingchuan.ma16@imperial.ac.uk;

stavros.petridis04@imperial.ac.uk; tingting.zhu@eng.ox.ac.uk;

david.clifton@eng.ox.ac.uk;

Supplementary Note 1 - Datasets

Pre-processing

PhysioNet-2012. The PhysioNet-2012 dataset [2] consists of 8,000 ICU-staying records that are publicly available to study issues of in-hospital mortality. A total of 42 variables are presented in each stay, each documented at least once during the first 48 hours after ICU entrance. 37 of those variables are time series with multiple observations during the 48-hour session, while 6 are general descriptors collected once on ICU admissions. “Weight” is both a general descriptor (measured at admission) and a time series (recorded hourly). We convert each time-series variable into a 48-Dimensional vector,

Supplementary Table 1: The clinical variables in PhysioNet-2012. We create one or multiple 48-D vectors for each variable. We apply one-hot encoding to represent “Gender” and “ICUType”, and we specify the categorical value with “→”. “Counts(Vec.)” refer to the variable count post-pending number of vectors after pre-processing. Each ICU stay leads to a matrix of size 48×47 with “in-hospital death” as the outcome label.

Clinical Variables		Type	Count(Vec.)
<ul style="list-style-type: none"> • Albumin • Blood urea nitrogen • Glasgow Coma Score • Serum potassium • Serum sodium • Serum creatinine • Bilirubin • Mechanical ventilation respiration • Alanine transaminase • Invasive systolic arterial blood pressure • Non-invasive diastolic arterial blood pressure • Serum bicarbonate • Non-invasive systolic arterial blood pressure • Arterial pH • Platelets • Troponin-I • Heart rate • O2 saturation in hemoglobin • Weight 	<ul style="list-style-type: none"> • Alkaline phosphatase • Cholesterol • Serum glucose • Lactate • Urine output • Temperature • Fractional inspired O2 • Partial pressure of arterial CO2 • Aspartate transaminase • Invasive diastolic arterial blood pressure • Non-invasive mean arterial blood pressure • Hematocrit • Invasive mean arterial blood pressure • Serum magnesium • Respiration rate • Troponin-T • White blood cell count • Partial pressure of arterial O2 	Time series	37(37)
<ul style="list-style-type: none"> • Age • Height • ICUType→Surgical ICU • ICUType→Cardiac Surgery Recovery Unit 	<ul style="list-style-type: none"> • Gender→Female • Gender→Male • ICUType→Medical ICU • ICUType→Coronary Care Unit 	General descriptor	4(8)
<ul style="list-style-type: none"> • SAPS-I 	<ul style="list-style-type: none"> • SOFA 	Scoring	2(2)
<ul style="list-style-type: none"> • In-Hospital Death 		Outcome	1(1)

each value depicting the state of that hour-session. We cast each general descriptor into 48-D vectors of constant temporal values (“RecordID” are not included). Notably, we follow the one-hot encoding strategy for the two categorical variables “Gender” and “ICUType”, with two 48-D binary vectors describing the former and four for the latter. Two extra scoring variables, SAPS-I [3] and SOFA [4], are also employed and converted into two 48-channel vectors, respectively. We stack all vectors from an ICU stay into a representative matrix of shape 48×47 , in which 48 corresponds to hours and 47 refers to the features. The outcome is a binary variable “in-hospital death” indicating whether the patient is a survivor (negative) or died in the hospital (positive), with a total of 6,878 negative samples and 1,122 positive ones, respectively. Supplementary Table 1 summarises the clinical variables of PhysioNet-2012.

Supplementary Table 2: The clinical variables in MIMIC-III. For each variable, we create one or multiple 48-D vectors with imputed values following [1]. We apply one-hot encoding to represent each categorical variable, and we detail the categorical value using “→”. Those imputation-indicating mask vectors are seen as inputs. “GCS” refers to “Glasgow coma scale”, while “verb. resp.” is “verbal response”. Each ICU stay leads to a 48×60 matrix with “in-hospital death” as the outcome.

Clinical Variables		Type	Count (Vec.)
<ul style="list-style-type: none"> • Diastolic blood pressure • Fraction inspired oxygen • Glucose • Heart Rate • Height • Mean blood pressure 	<ul style="list-style-type: none"> • Oxygen saturation • Respiratory rate • Systolic blood pressure • Temperature • Weight • pH 	Continuous	12(12)
<ul style="list-style-type: none"> • Capillary refill rate → 0 • GCS eye opening → To speech • GCS eye opening → To Pain • GCS eye opening → Spontaneously • GCS verb. resp. → Incomprehensible sounds • GCS verb. resp. → No Response • GCS motor response → Abnormal extension • GCS motor response → No Response • GCS motor response → Localizes Pain • GCS total → 3 • GCS total → 4 • GCS total → 5 • GCS total → 6 • GCS total → 7 • GCS total → 8 • GCS total → 9 	<ul style="list-style-type: none"> • Capillary refill rate → 1 • GCS eye opening → None • GCS verb. resp. → Confused • GCS eye opening → No Response • GCS verb. resp. → Inappropriate Words • GCS verb. resp. → Oriented • GCS motor response → Abnorm flexion • GCS motor response → Flex-withdraws • GCS motor response → Obeys Commands • GCS total → 10 • GCS total → 11 • GCS total → 12 • GCS total → 13 • GCS total → 14 • GCS total → 15 	Categorical	5(31)
<ul style="list-style-type: none"> • mask → Capillary refill rate • mask → Fraction inspired oxygen • mask → GCS motor response • mask → GCS total • mask → Heart Rate • mask → Mean blood pressure • mask → Respiratory rate • mask → Temperature • mask → pH 	<ul style="list-style-type: none"> • mask → GCS eye opening • mask → Diastolic blood pressure • mask → GCS verb. resp. • mask → Glucose • mask → Height • mask → Oxygen saturation • mask → Systolic blood pressure • mask → Weigh 	Mask	17(17)
<ul style="list-style-type: none"> • In-Hospital Death 		Outcome	1(1)

MIMIC-III. We generally follow [1] to pre-process the MIMIC-III dataset [5, 6]. In particular, the MIMIC-III dataset used in this work comprises 21,156 ICU stays of 17 clinical variables selected from tables “CHARTEVENTS” and “LBEVENTS” (see [5] for details of those tables). Those variables are documented during the first 48 hours of ICU admission and can be divided into 5 categorical and 12 continuous. Each continuous variable is converted into a 48-D numeric vector, and we encode each categorical variable into

one-hot vectors. All missing values are imputed following [1], and we have attached the 17 binary mask vectors indicating whether a variable’s values are true or imputed as extra input information. After pre-processing, we can generate 60 48-D vectors representing each ICU stay, i.e., a 48×60 matrix. We consider the “in-hospital mortality” as the outcome label with 18357 negative (“survivor”) and 2799 positive (“died in the hospital”) cases. Supplementary Table 2 illustrates all clinical variables in MIMIC-III.

Coswara. The Coswara dataset [7] consists of 1,368 breathing sounds sampled from participants with polymerase chain reaction (PCR) test results, and the outcome is diagnosing coronavirus-19 (Covid-19). The duration of an original sound is approximately 3 to 8 seconds at 48-kHz frequency, and we crop a 3-second region of the highest acoustic intensity per sample to unify the time length. Then we employ a short-term Fourier transform (STFT) with a 100ms FFT window of 50% overlap to extract the 64 log mel-bands Mel-spectrogram. This extraction results in a 94×64 representation matrix for each breathing sound, and 94 and 64 are the temporal and acoustic dimensions, respectively. This dataset contains 948/420 samples with positive/negative PCR results.

Dataset splits

Supplementary Table 3: Number of samples (number of positive/negative instances) in the train, validation, and test sets across three datasets.

Dataset	Train	Validation	Test
PhysioNet-2012	5,120 (728/4,392)	1,280 (167/1,113)	1,600 (227/1,373)
MIMIC-III	14,698 (1,989/12,709)	3,222 (436/2,786)	3,236 (374/2,862)
Coswara	987 (683/304)	175 (121/54)	206 (144/62)

Across three datasets, we split the data into train, validation, and test sets. The train set is used to learn the condensed data and to train DNNs, while the validation and test is used for evaluating performance of DNNs. Supplementary Table 3 provides an overview of the data splits used in this paper.

Supplementary Note 2 - Deep Neural Networks

Network Architectures

We select a cohort of 11 prevalent DNNs for time-series data to evaluate the deep-learning utility of original and condensed train sets. Those 11 DNNs are from a total of five neural network families: multi-scale temporal convolution networks (MS-TCNs) [8], transformers (TRSFs) [9], vision transformers (ViTs) [10], long short term memory networks (LSTMs) [11], and recurrent neural networks (RNNs) [12].

Multi-scale temporal convolution networks. Multi-scale temporal convolution networks (MS-TCNs) [8] are a variant of temporal convolution networks (TCNs) [14] and have achieved state-of-the-art performance in various computer vision tasks such as lip-reading. TCNs utilise 1D causal convolutions to analyse the temporal information in time-serial data, and MS-TCNs improve their architectures by introducing multi-scale convolutions of varying kernel sizes to better reflect the temporal information of different scales. We employ three MS-TCNs in this work, denoted as TCN- α , TCN- β , and TCN- γ . All networks consist of two temporal convolutional (TC) layers, followed by a temporal pooling and a fully connected (FC) layer. Each TC layer in TCN- α comprises three branches of kernel sizes 3, 5, and 7, respectively, and each branch’s hidden neuron number is set to 64. For TCN- β , each TC layer only contains a single convolutional branch of kernel size 3 with hidden dimension 64. Every TC layer in TCN- γ is set to be a double-branch structure with 64 hidden neurons and a kernel size of 3 and 5 in each branch. Supplementary Table 4 demonstrates the architectures of TCN- α , TCN- β , and TCN- γ .

Transformers and vision transformers. Transformers (TRSFs) [9] is initially proposed to address Natural Language Processing (NLP) issues. The self-attention mechanism enables transformers to capture the input signals’ global dependencies; therefore, they are extensively applied in various fields with impressive results. The original transformer [9] is constituted of one encoder and one decoder. In this work, we employ the transformer encoder to extract the embedding of time-serial data and discard the decoder. We mainly examine two transformer encoders of varying architectures, TRSF- α and TRSF- β . Both networks comprise two multi-headed self-attention (MSA) layers followed by a temporal pooling and a multi-layer perceptron (MLP) head of two FC layers. We ignore the positional embedding for simplicity. In TRSF- α , we set each MSA layer to include 16 self-attention heads, and each head consists of 64 attention channels. The hidden neurons in MLP are set to 64. Each MSA layer in TRSF- β comprises 4 attention heads of 256 channels, and the hidden dimension of its MLP is 128.

Vision transformers (ViTs) [10] are a variant of transformers designed for image recognition. Dividing each image into patches and linearly projecting

Supplementary Table 4: The architectures of TCN- α , TCN- β , and TCN- γ . The kernel size is post-pended to each *Conv1D* operation, and the dropout rate is also indicated following each *Dropout*. We apply PReLU [13] as the main activation function. “RC i →” refers to the starting of the i -th residual connection, and “RC i ←” for the ending. “Concat.” stands for channel-wise concatenation, while “Chomp1D” is the causal convolution implementation [14].

Layer	Branch1	TCN- α Branch2	Branch3	TCN- β	TCN- γ Branch1	Branch2
1		RC1→		RC1→	RC1→	
	Conv1D(3)	Conv1D(5)	Conv1D(7)	Conv1D(3)	Conv1D(3)	Conv1D(5)
	BatchNorm	BatchNorm	BatchNorm	BatchNorm	BatchNorm	BatchNorm
	Chomp1D	Chomp1D	Chomp1D	Chomp1D	Chomp1D	Chomp1D
	PReLU	PReLU	PReLU	PReLU	PReLU	PReLU
	Concat. & Dropout(0.5)			Dropout(0.5)	Concat. & Dropout(0.5)	
	Conv1D(3)	Conv1D(5)	Conv1D(7)	Conv1D(3)	Conv1D(3)	Conv1D(5)
	BatchNorm	BatchNorm	BatchNorm	BatchNorm	BatchNorm	BatchNorm
	Chomp1D	Chomp1D	Chomp1D	Chomp1D	Chomp1D	Chomp1D
	PReLU	PReLU	PReLU	PReLU	PReLU	PReLU
Concat. & Dropout(0.5)			Dropout(0.5)	Concat. & Dropout(0.5)		
	Conv1D(1)		Conv1D(1)		Conv1D(1)	
	RC1←		RC1←		RC1←	
	PReLU		PReLU		PReLU	
2		RC2→		RC2→		RC2→
	Conv1D(3)	Conv1D(5)	Conv1D(7)	Conv1D(3)	Conv1D(3)	Conv1D(5)
	BatchNorm	BatchNorm	BatchNorm	BatchNorm	BatchNorm	BatchNorm
	Chomp1D	Chomp1D	Chomp1D	Chomp1D	Chomp1D	Chomp1D
	PReLU	PReLU	PReLU	PReLU	PReLU	PReLU
	Concat. & Dropout(0.5)			Dropout(0.5)	Concat. & Dropout(0.5)	
	Conv1D(3)	Conv1D(5)	Conv1D(7)	Conv1D(3)	Conv1D(3)	Conv1D(5)
	BatchNorm	BatchNorm	BatchNorm	BatchNorm	BatchNorm	BatchNorm
	Chomp1D	Chomp1D	Chomp1D	Chomp1D	Chomp1D	Chomp1D
	PReLU	PReLU	PReLU	PReLU	PReLU	PReLU
Concat. & Dropout(0.5)			Dropout(0.5)	Concat. & Dropout(0.5)		
	Conv1D(1)		Conv1D(1)		Conv1D(1)	
	RC2←		RC2←		RC2←	
	PReLU		PReLU		PReLU	
3		Pooling		Pooling		Pooling
		Linear		Linear		Linear
		Sigmoid		Sigmoid		Sigmoid

patches into sequential embedding, ViTs can be used to analyse images with state-of-the-art performance. ViTs also differ from transformers in obtaining the sequence representation. A learnable token is pre-appended to the input and its corresponding part at the output side is fed into the MLP. We discard the linear projection component in this work and feed time-serial data directly into the ViT encoder. A total of two ViTs with different architectures are inspected, ViT- α and ViT- β . Both ViTs contain four MSA layers, and

Supplementary Table 5: The architectures of TRSF- α , TRSF- β , ViT- α , and ViT- β . “MSA” refers to the Multi-head Self-attention Layer, and the head number and attention channel are post-pended. “[token] \leftarrow ” refers to appending a learning token to input, and “[token] \rightarrow ” means getting the token at output side. “F.F.” stands for the feed-forward layer and consists of two FC layers. We apply GELU [15] as the major activation function.

Layer	TRSF- α	TRSF- β	ViT- α	ViT- β
1	RC1a \rightarrow	RC1a \rightarrow	[token] \leftarrow RC1a \rightarrow	[token] \leftarrow RC1a \rightarrow
	LayerNorm	LayerNorm	LayerNorm	LayerNorm
	MSA(16,64)	MSA(4,256)	MSA(16,64)	MSA(4,256)
	RC1a \leftarrow	RC1a \leftarrow	RC1a \leftarrow	RC1a \leftarrow
	RC1b \rightarrow	RC1b \rightarrow	RC1b \rightarrow	RC1b \rightarrow
	LayerNorm	LayerNorm	LayerNorm	LayerNorm
	F.F.	F.F.	F.F.	F.F.
RC1b \leftarrow	RC1b \leftarrow	RC1b \leftarrow	RC1b \leftarrow	
2	RC2a \rightarrow	RC2a \rightarrow	RC2a \rightarrow	RC2a \rightarrow
	LayerNorm	LayerNorm	LayerNorm	LayerNorm
	MSA(16,64)	MSA(4,256)	MSA(16,64)	MSA(4,256)
	RC2a \leftarrow	RC2a \leftarrow	RC2a \leftarrow	RC2a \leftarrow
	RC2b \rightarrow	RC2b \rightarrow	RC2b \rightarrow	RC2b \rightarrow
	LayerNorm	LayerNorm	LayerNorm	LayerNorm
	F.F.	F.F.	F.F.	F.F.
RC2b \leftarrow	RC2b \leftarrow	RC2b \leftarrow	RC2b \leftarrow	
3	Pooling	Pooling	RC3a \rightarrow	RC3a \rightarrow
	LayerNorm	LayerNorm	LayerNorm	LayerNorm
	Linear	Linear	MSA(16,64)	MSA(4,256)
	GELU	GELU	RC3a \leftarrow	RC3a \leftarrow
	Dropout(0.5)	Dropout(0.5)	RC3b \rightarrow	RC3b \rightarrow
	Linear	Linear	LayerNorm	LayerNorm
	Sigmoid	Sigmoid	F.F.	F.F.
RC3b \leftarrow	RC3b \leftarrow	RC3b \leftarrow	RC3b \leftarrow	
4	N/A	N/A	RC4a \rightarrow	RC4a \rightarrow
			LayerNorm	LayerNorm
			MSA(16,64)	MSA(4,256)
			RC4a \leftarrow	RC4a \leftarrow
			RC4b \rightarrow	RC4b \rightarrow
			LayerNorm	LayerNorm
			F.F.	F.F.
		RC4b \leftarrow	RC4b \leftarrow	
5			[token] \rightarrow	[token] \rightarrow
			LayerNorm	LayerNorm
			Linear	Linear
			GELU	GELU
			Dropout(0.5)	Dropout(0.5)
			Linear	Linear
			Sigmoid	Sigmoid

the corresponding output of the learnable token is fed into an MLP with two FC layers, while the positional embedding is also omitted for simplicity. ViT- α possesses 16 self-attention heads with 64 channels per MSA layer, while each MSA of ViT- β is made up of 4 heads of 128 attention channels. Supplementary Table 5 illustrates the architectures of TRSF- α , TRSF- β , ViT- α , and

Supplementary Table 6: The architectures of LSTM- α , LSTM- β , RNN- α , and RNN- β . We post-append the hidden state units to each ‘‘RNN Cell’’ and ‘‘LSTM Cell’’.

Layer	LSTM- α	LSTM- β	RNN- α	RNN- β
1	LSTM Cell (256)	LSTM Cell (128)	RNN Cell (256)	RNN Cell (128)
2	Linear Sigmoid	Linear Sigmoid	Linear Sigmoid	Linear Sigmoid

ViT- β in details.

LSTMs and RNNs. Long short term memory networks (LSTMs) [11] and recurrent neural networks (RNNs) [12] are both recurrent-based networks but with varying implementations. RNNs are known to be unable to capture the long-term temporal dependency within data due to their naive architectures, while LSTMs improve this limitation by introducing more sophisticated gating mechanisms. In this work, we apply two LSTMs and two RNNs denoted as LSTM- α and LSTM- β , RNN- α , and RNN- β , respectively. Across the four architectures, the time-series data is fed into one recurrent layer, either LSTM-based or RNN-based, followed by an FC layer for final predictions. LSTM- α differs from LSTM- β in that the recurrent layer of the former consists of a hidden state of 256 units, while the latter comprises 128 instead. We set the dimension of the hidden state in RNN- α ’s recurrent layer to be 256, and 128 for RNN- β . Supplementary Table 6 explain the architectures of LSTM- α and LSTM- β , RNN- α , and RNN- β .

Training settings

Supplementary Table 7: The training setting for 11 DNNs across three datasets. We use BCE loss and Adam optimiser for all experiments. “Init. LR” refers to the initial learning rate for Adam optimiser, and “ $\min(64, |\mathcal{C}|)$ ” stands for using the smaller of 64 and $|\mathcal{C}|$ (size of condensed set) as the batch size.

Dataset	Train data	Hyper-parameters		Epochs
		Batch Size	Init. LR	
PhysioNet-2012	Original	64	5×10^{-4}	30
	Condensed	$\min(64, \mathcal{C})$		
MIMIC-III	Original	64	5×10^{-5}	20
	Condensed			
Coswara	Original	64	1×10^{-4}	30
	Condensed	$\min(64, \mathcal{C})$		

Across all three datasets, we trained all 11 networks on the original train set and its condensed versions to evaluate the deep-learning utility preserved by DC. The binary cross entropy (BCE) loss is employed to train all DNNs, and we apply Adam [16] optimiser for all experiments with varying initial learning rates on different datasets. We also perform a data standardisation (subtracted by mean and divided by STD) for numeric input data before feeding it into DNNs. The detailed training hyper-parameters are summarised in Supplementary Table 7. Note that those settings should be distinguished from the hyper-parameters of learning condensed data described in Section “Methods” of the main manuscript.

Supplementary Note 3 - Results

AUCs of 11 DNNs

Supplementary Table 8: The AUC of DNNs trained on original and condensed sets across all 3 datasets and 11 networks. We repeat each training session for five times and report the average AUC with STD on the test set. “AVG” refers to the average AUC of all sessions.

Dataset	Train data (samples)	Test AUC (SD)			
		TCN- α	TCN- β	TCN- γ	ViT- α
PhysioNet-2012	Ori.(5120)	0.854 (0.005)	0.858 (0.005)	0.852 (0.006)	0.854 (0.003)
	Con.(80)	0.806 (0.003)	0.800 (0.003)	0.804 (0.006)	0.798 (0.008)
	Con.(40)	0.813 (0.003)	0.804 (0.005)	0.808 (0.005)	0.788 (0.007)
	Con.(20)	0.808 (0.006)	0.807 (0.002)	0.808 (0.002)	0.806 (0.011)
MIMIC-III	Ori.(14698)	0.843 (0.004)	0.833 (0.002)	0.845 (0.001)	0.835 (0.002)
	Con.(1200)	0.756 (0.001)	0.750 (0.006)	0.756 (0.002)	0.743 (0.011)
	Con.(800)	0.748 (0.002)	0.736 (0.009)	0.747 (0.000)	0.744 (0.007)
	Con.(400)	0.740 (0.006)	0.704 (0.021)	0.742 (0.007)	0.740 (0.008)
Coswara	Ori.(987)	0.729 (0.017)	0.750 (0.007)	0.740 (0.018)	0.727 (0.019)
	Con.(80)	0.646 (0.010)	0.635 (0.006)	0.641 (0.002)	0.637 (0.030)
	Con.(40)	0.645 (0.007)	0.636 (0.008)	0.650 (0.014)	0.626 (0.021)
	Con.(20)	0.647 (0.006)	0.633 (0.005)	0.651 (0.012)	0.590 (0.022)
		ViT- β	TRSF- α	TRSF- β	LSTM- α
PhysioNet-2012	Ori.(5120)	0.851 (0.005)	0.853 (0.003)	0.843 (0.016)	0.869 (0.003)
	Con.(80)	0.798 (0.010)	0.781 (0.006)	0.788 (0.005)	0.815 (0.004)
	Con.(40)	0.797 (0.006)	0.779 (0.007)	0.784 (0.011)	0.816 (0.007)
	Con.(20)	0.794 (0.014)	0.789 (0.007)	0.787 (0.004)	0.804 (0.005)
MIMIC-III	Ori.(14698)	0.830 (0.003)	0.835 (0.001)	0.832 (0.004)	0.849 (0.004)
	Con.(1200)	0.745 (0.007)	0.742 (0.005)	0.743 (0.005)	0.776 (0.003)
	Con.(800)	0.741 (0.006)	0.734 (0.006)	0.742 (0.006)	0.777 (0.011)
	Con.(400)	0.737 (0.005)	0.735 (0.009)	0.737 (0.008)	0.770 (0.010)
Coswara	Ori.(987)	0.738 (0.020)	0.732 (0.017)	0.741 (0.020)	0.739 (0.005)
	Con.(80)	0.634 (0.009)	0.642 (0.019)	0.629 (0.017)	0.654 (0.006)
	Con.(40)	0.614 (0.017)	0.630 (0.034)	0.643 (0.026)	0.654 (0.007)
	Con.(20)	0.618 (0.029)	0.603 (0.024)	0.602 (0.028)	0.663 (0.013)
		AVG	LSTM- β	RNN- α	RNN2- β
PhysioNet-2012	Ori.(5120)	0.858 (0.011)	0.873 (0.003)	0.864 (0.009)	0.872 (0.005)
	Con.(80)	0.804 (0.014)	0.817 (0.011)	0.820 (0.004)	0.820 (0.006)
	Con.(40)	0.804 (0.016)	0.813 (0.012)	0.822 (0.008)	0.815 (0.011)
	Con.(20)	0.803 (0.012)	0.816 (0.005)	0.811 (0.013)	0.804 (0.015)
MIMIC-III	Ori.(14698)	0.840 (0.007)	0.844 (0.002)	0.847 (0.001)	0.845 (0.002)
	Con.(1200)	0.756 (0.014)	0.774 (0.007)	0.768 (0.004)	0.761 (0.013)
	Con.(800)	0.750 (0.014)	0.761 (0.006)	0.757 (0.006)	0.761 (0.012)
	Con.(400)	0.741 (0.019)	0.749 (0.016)	0.760 (0.007)	0.738 (0.012)
Coswara	Ori.(987)	0.737 (0.017)	0.735 (0.007)	0.753 (0.005)	0.721 (0.014)
	Con.(80)	0.642 (0.016)	0.651 (0.011)	0.648 (0.005)	0.640 (0.013)
	Con.(40)	0.641 (0.021)	0.652 (0.012)	0.658 (0.009)	0.645 (0.008)
	Con.(20)	0.632 (0.030)	0.653 (0.010)	0.648 (0.009)	0.647 (0.011)

Effects of changing temporal dimension in DC

Supplementary Table 9: The effects of different temporal dimensions of condensed samples across 3 datasets. $|\mathcal{C}|$ refers to the number of samples in the condensed set, while “ T (Ori.)” and “ T (Con.)” are abbreviations of the time dimension in the original and condensed samples, respectively. Reducing T^* can further compress the data volumes without significantly affecting the test AUCs, reflecting high flexibility in size control using DC.

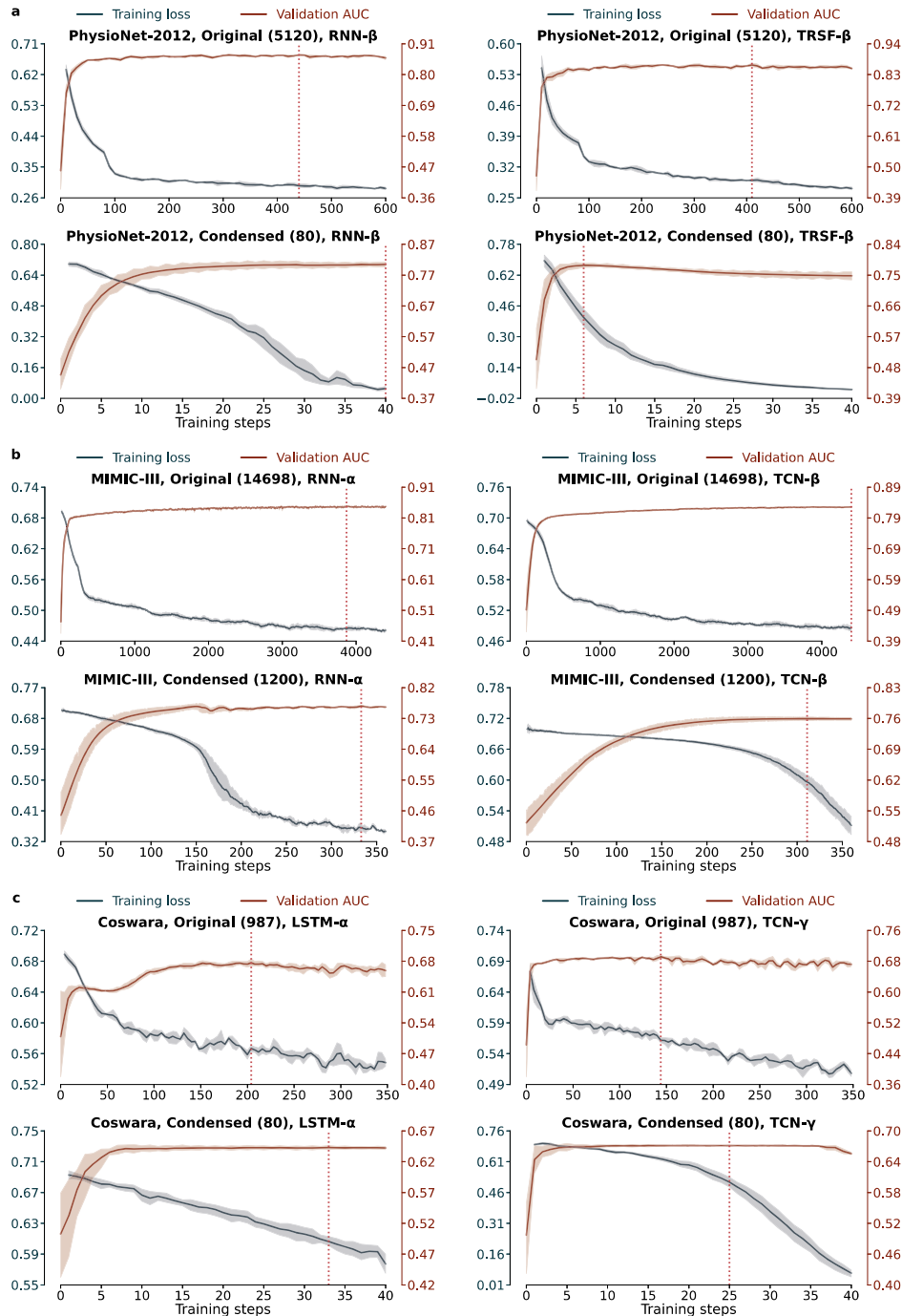
Dataset	$ \mathcal{C} $	Temporal Dimension		Sizes (MBs)	Test AUC (SD)
		T (Ori.)	T^* (Con.)		
PhysioNet-2012	80	48	48	0.69	0.804 (0.014)
			36	0.52	0.799 (0.015)
			24	0.34	0.801 (0.016)
			12	0.17	0.801 (0.016)
MIMIC-III	1200	48	48	13.18	0.756 (0.014)
			36	9.89	0.745 (0.017)
			24	6.59	0.747 (0.017)
			12	3.30	0.746 (0.018)
Coswara	80	96	96	1.88	0.642 (0.016)
			64	1.25	0.639 (0.021)
			32	0.63	0.631 (0.034)
			16	0.31	0.632 (0.030)

Across the manuscript, we pre-define each condensed sample to retain the size of the original one, i.e., for original instances $\mathbf{x} \in \mathbb{R}^{T \times F}$ where T and F correspond to the temporal and feature dimension, we will learn condensed samples of the same shape $\mathbf{c} \in \mathbb{R}^{T \times F}$. In principle, however, we can set the condensed sample to have inconsistent sizes as the original insofar as the embedding distributions between them can still be matched in DC. In this work, we employ 11 DNNs as the embedding function, while all architectures can accept input with an arbitrary temporal dimension. That is, we can define condensed samples $\mathbf{c} \in \mathbb{R}^{T^* \times F}$ where $T^* \neq T$ or $T^* = T$.

We investigate the effects of different temporal dimensions (TDs) in condensed samples in Supplementary Table 9. We can discover that using a smaller T^* can further compress the data volumes without significantly affecting the test AUCs. This observation reflects an extra advantage of DC: the flexibility in size control. After choosing $|\mathcal{C}| \ll |\mathcal{O}|$, we could further compress the sizes of condensed data by picking a $T^* < T$ at the cost of slightly decreased accuracy.

Learning Curves

Supplementary Figure 1: Learning curves of different networks trained on the original and condensed data across 3 datasets. The red-dotted line indicates the step of convergence. **a**, RNN- β and TRSF- β on PysioNet-2012. **b**, RNN- α and TCN- β on MIMIC-III. **c**, LSTM- α and TCN- γ on Coswara. The convergence rates of DNNs trained on the condensed data significantly outperform the same networks trained on the original.



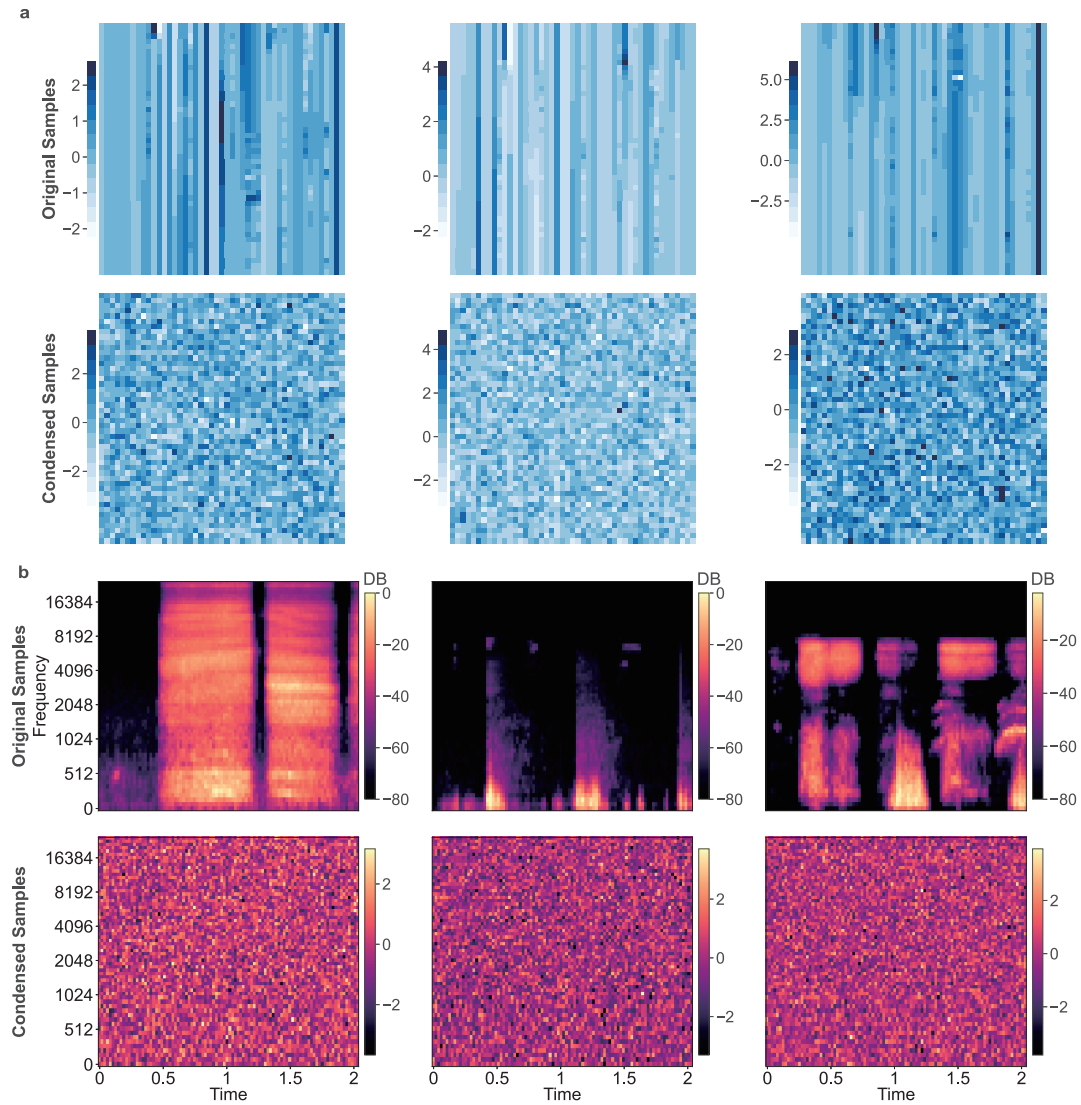
Learning time of DC

Supplementary Table 10: Training time required to learn condensed sets of different sizes across 3 datasets. We measure the duration (minutes) of each DC learning session of 24,000 iterations on an NVIDIA GeForce RTX 3060 graphic card. All condensed datasets can be learned within approximately 1 hour.

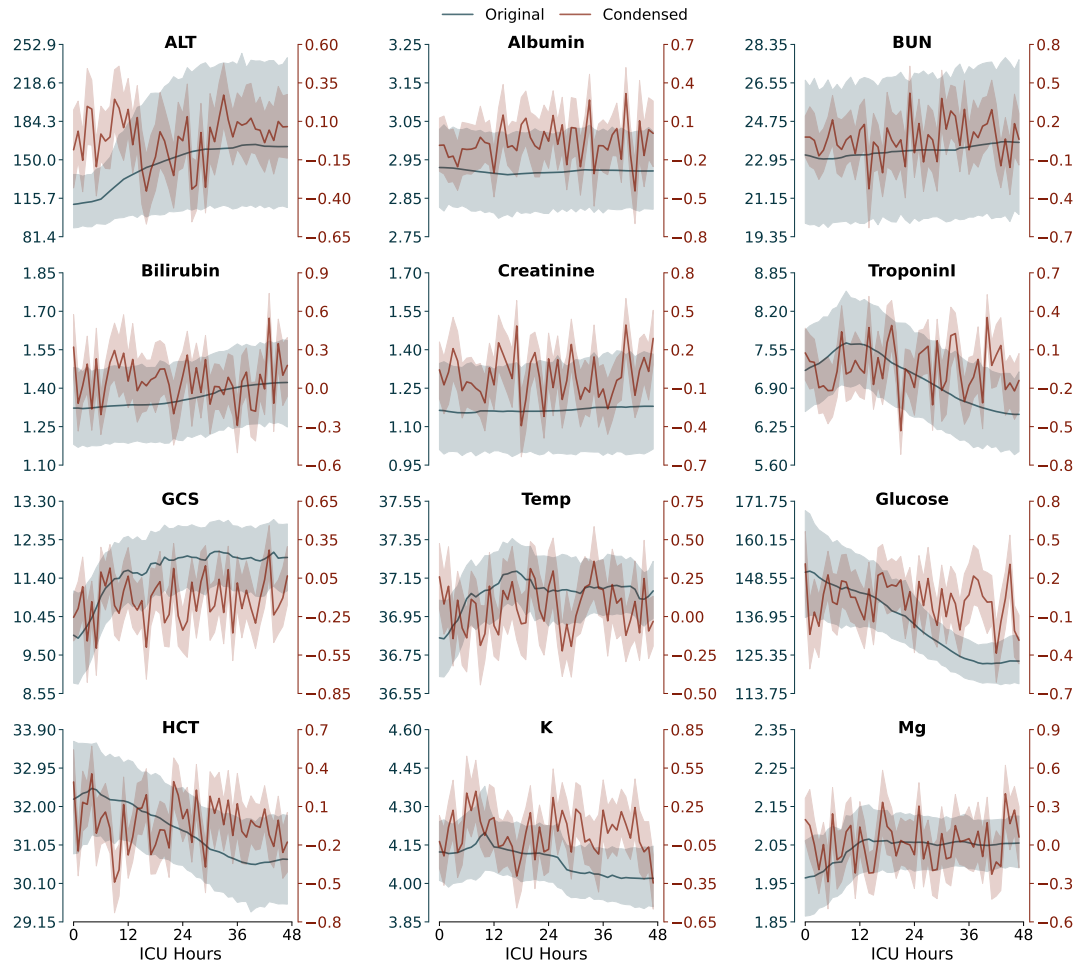
Dataset (samples)	Condensed size	DC Time (min)
PhysioNet-2012 (5120)	80	18.3
	40	16.9
	20	16.2
MIMIC-III (14698)	1200	61.8
	800	46.0
	400	30.6
Coswara (987)	80	31.1
	40	28.2
	20	27.4

Data Visualisation

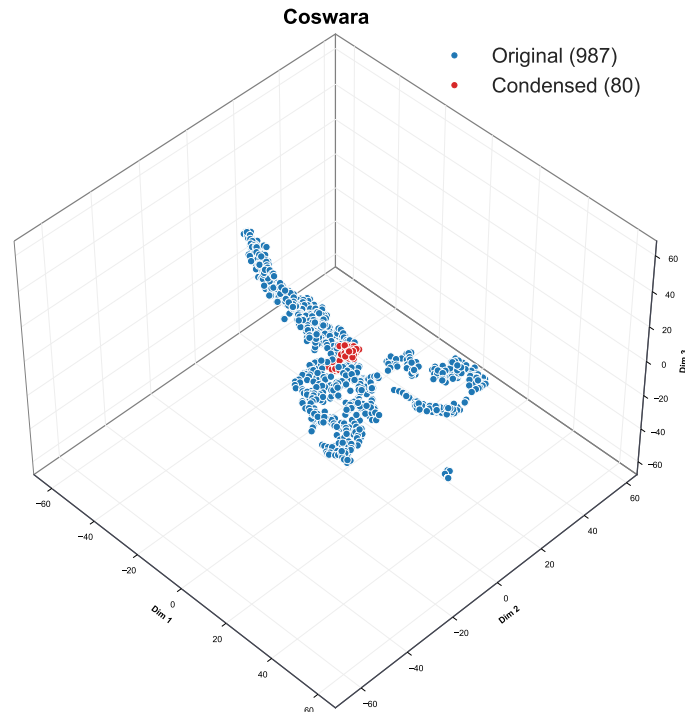
Supplementary Figure 2: a, the heatmaps of three original and three condensed samples randomly picked from PhysioNet. **b**, the mel-spectrogram plots of three random audio segments and three random condensed samples on Coswara. Condensed instances behave like random noises without regular patterns in the original ones.



Supplementary Figure 3: The 48-hour trends of 12 additional clinical variables from PhysioNet-2012 computed from 80 original and 80 condensed instances, respectively. Those variables are: Alanine transaminase (“ALT”), Albumin, Blood urea nitrogen (“BUN”), Bilirubin, Serum creatinine (“Creatinine”), Troponin-I, Glasgow Coma Score (“GCS”), Temperature (“Temp”), Serum glucose (“Glucose”), Hematocrit (“HCT”), Serum potassium (“K”), and Serum magnesium (“Mg”).



Supplementary Figure 4: The 3D distributions of 987 original and 80 condensed samples embedded into 3D with t-SNE on Coswara.



References

- [1] Harutyunyan, H., Khachatryan, H., Kale, D.C., Ver Steeg, G., Galstyan, A.: Multitask learning and benchmarking with clinical time series data. *Scientific data* **6**(1), 1–18 (2019)
- [2] Silva, I., Moody, G., Scott, D.J., Celi, L.A., Mark, R.G.: Predicting in-hospital mortality of icu patients: The physionet/computing in cardiology challenge 2012. In: 2012 Computing in Cardiology, pp. 245–248 (2012). IEEE
- [3] Le Gall, J.-R., Loirat, P., Alperovitch, A., Glaser, P., Granthil, C., Mathieu, D., Mercier, P., Thomas, R., Villers, D.: A simplified acute physiology score for icu patients. *Critical care medicine* **12**(11), 975–977 (1984)
- [4] Ferreira, F.L., Bota, D.P., Bross, A., Mélot, C., Vincent, J.-L.: Serial evaluation of the sofa score to predict outcome in critically ill patients. *Jama* **286**(14), 1754–1758 (2001)
- [5] Johnson, A.E., Pollard, T.J., Shen, L., Lehman, L.-w.H., Feng, M., Ghassemi, M., Moody, B., Szolovits, P., Anthony Celi, L., Mark, R.G.:

- Mimic-iii, a freely accessible critical care database. *Scientific data* **3**(1), 1–9 (2016)
- [6] Johnson, A., Pollard, T., Mark, R.: Mimic-iii clinical database (version 1.4). *PhysioNet* **10**, 2–26 (2016)
- [7] Sharma, N., Krishnan, P., Kumar, R., Ramoji, S., Chetupalli, S., Nirmala, R., Kumar Ghosh, P., Ganapathy, S.: Coswara-a database of breathing, cough, and voice sounds for covid-19 diagnosis. In: *Proceedings of the Annual Conference of the International Speech Communication Association, INTERSPEECH*, vol. 2020, pp. 4811–4815 (2020). International Speech Communication Association
- [8] Martinez, B., Ma, P., Petridis, S., Pantic, M.: Lipreading using temporal convolutional networks. In: *ICASSP 2020-2020 IEEE International Conference on Acoustics, Speech and Signal Processing (ICASSP)*, pp. 6319–6323 (2020). IEEE
- [9] Vaswani, A., Shazeer, N., Parmar, N., Uszkoreit, J., Jones, L., Gomez, A.N., Kaiser, Ł., Polosukhin, I.: Attention is all you need. *Advances in neural information processing systems* **30** (2017)
- [10] Dosovitskiy, A., Beyer, L., Kolesnikov, A., Weissenborn, D., Zhai, X., Unterthiner, T., Dehghani, M., Minderer, M., Heigold, G., Gelly, S., Uszkoreit, J., Houlsby, N.: An image is worth 16x16 words: Transformers for image recognition at scale. In: *International Conference on Learning Representations* (2021). <https://openreview.net/forum?id=YicbFdNTTy>
- [11] Hochreiter, S., Schmidhuber, J.: Long short-term memory. *Neural computation* **9**(8), 1735–1780 (1997)
- [12] Hopfield, J.J.: Neural networks and physical systems with emergent collective computational abilities. *Proceedings of the national academy of sciences* **79**(8), 2554–2558 (1982)
- [13] He, K., Zhang, X., Ren, S., Sun, J.: Delving deep into rectifiers: Surpassing human-level performance on imagenet classification. In: *Proceedings of the IEEE International Conference on Computer Vision*, pp. 1026–1034 (2015)
- [14] Bai, S., Kolter, J.Z., Koltun, V.: An empirical evaluation of generic convolutional and recurrent networks for sequence modeling. *arXiv preprint arXiv:1803.01271* (2018)
- [15] Hendrycks, D., Gimpel, K.: Gaussian error linear units (gelus). *arXiv preprint arXiv:1606.08415* (2016)

- [16] Kingma, D.P., Ba, J.: Adam: A method for stochastic optimization. arXiv preprint arXiv:1412.6980 (2014)